Site Characterisation for Geological Storage of Carbon Dioxide: Examples of Potential Sites from the North West Shelf, Australia

Catherine M. Gibson-Poole

B.Sc. (Hons.) Geology – Royal Holloway University of London, UK

M.Sc. Micropalaeontology – University of Southampton, UK

Australian School of Petroleum

The University of Adelaide

This thesis is submitted in fulfilment of the requirements of Doctor of Philosophy in the Faculty of Science, The University of Adelaide

August 2009

CHAPTER 6. CASE STUDY 2: BARROW SUB-BASIN

6.1 INTRODUCTION

Prior to site selection, the GEODISC™ Program undertook a regional characterisation process to assess sites across Australia for their potential for geological storage of CO_2 (Bradshaw *et al.*, 2000). The potential sites, termed Environmentally Sustainable Sites for CO_2 Injection (ESSCI), were assessed in terms of their location logistics, injectivity potential, containment security, likely storage capacity and proximity to existing natural resources. The outcome of the regional characterisation was a ranked listing of potential ESSCIs with the most appropriate parameters for large-scale CO_2 injection (Bradshaw *et al.*, 2000; Bradshaw *et al.*, 2002).

The Muderong Shale Subcrop ESSCI in the Barrow Sub-basin, offshore northwest Australia (UEI 4/UEI 9 of Bradshaw *et al.*, 2000), was selected to proceed to detailed site-specific characterisation, as it ranked highly in all assessment criteria except the possibility of interference with an active petroleum system. It was also selected to provide a conceptual example of a stratigraphically complex site, where the interfingering of basin floor fan lobes with up-dip continental slope and transgressive greensand deposits may be an important influence on the CO_2 migration pathways and have potential for stratigraphic trapping. The Muderong Shale Subcrop ESSCI comprises the Early Cretaceous Flag Sandstone as the initial CO_2 injection horizon, with up-dip migration within the Flag Sandstone and potentially into the Flacourt Formation and Mardie Greensand Member. The seal is provided by the regionally extensive Early Cretaceous Muderong Shale. This chapter documents the detailed geological site characterisation undertaken to assess the CO_2 storage potential of the Muderong Shale Subcrop ESSCI in the Barrow Sub-basin.

6.2 LOCATION AND GEOLOGICAL SETTING

The Barrow Sub-basin is a northeast-southwest trending trough within the Northern Carnarvon Basin, located offshore Western Australia on the North West Shelf (Figure 6.1). The northeast-trending Rankin Platform forms the northwestern margin of the Barrow Sub-basin and its southeastern limit is the northeast-trending Peedamullah Shelf. The transition from the shelf into the central trough is marked by the northeast-trending Flinders Fault System (Figure 6.1 and Figure 6.2). To the northeast and southwest the Barrow Sub-basin

abuts the Dampier and Exmouth sub-basins. Barrow Island is located on the north-northeast directed anticlinal Barrow Island Trend within the central trough (Kirk, 1985; Kopsen & McGann, 1985; Baillie & Jacobson, 1997; Romine *et al.*, 1997).

Figure 6.1 Location map of the Barrow Sub-basin, northwest Australia, and surrounding tectonic elements (modified after Baillie & Jacobson, 1997).

NOTE:
This figure is included on page 159 of the print copy of the thesis held in the University of Adelaide Library.

Figure 6.2 Structural cross-section of the Barrow Sub-basin (modified after Baillie & Jacobson, 1997). The location of the section is shown on Figure 6.1.

The study area for the potential CO_2 injection site is focussed over the Barrow Island anticline in the region between the Montebello Islands and Barrow Island and the oil and gas fields in Harriet-Campbell area to the east, covering a total study area of approximately 50 km by 75 km (Figure 6.3). The water depth ranges from 5 m at Plato-1 in the central area (near the Lowendal Islands) to 16.5 m in the south at Peck-1 and Hermite-1 to 60 m at Forrest-1A ST1 in the north. The Flag Sandstone is the main reservoir interval in the northern, central and eastern parts of the study area, which laterally grades into the Flacourt Formation to the south at Barrow Island. The depth to the base Flag Sandstone (maximum potential injection depth) ranges from 3000 m at Forrest-1A ST1 in the north to 1450 m at Georgette-1 in the southeast. Hydrocarbon production commenced in the mid 1960s on Barrow Island (Windalia Sandstone Member) and in the mid 1980s offshore at Harriet (Flag Sandstone); therefore there is quite a significant amount of infrastructure in place. This includes pipelines from the major producing fields (Alkimos, Campbell, Harriet, Rosette, Sinbad, Tanami and Wonnich) and processing facilities on Barrow Island and Varanus Island (near the Alkimos, Rosette and Tanami fields).

Figure 6.3 Location map of the study area, showing wells, oil and gas fields, and faults (fault traces redrawn after Hadson, 1995).

6.2.1 Structural and Stratigraphic Evolution

The sedimentary succession in the Carnarvon Basin extends from the Silurian to Recent. The Carnarvon Basin developed initially as a northerly-trending interior-fracture basin in the Silurian and evolved into an interior-sag basin in the early Devonian, continuing until the Late Permian (Hocking, 1988, 1990). Within the Northern Carnarvon Basin, remnants of this stage of basin evolution are only preserved on the Peedamullah Shelf and Candace Terrace. Following a hiatus in deposition, sedimentation recommenced in the Triassic into a broad interior-sag depocentre, with sediment sourced from the Pilbara Block to the east (Kirk, 1985; Kopsen & McGann, 1985).

The present day sub-basin configuration of the Northern Carnarvon Basin resulted mainly from the continental break-up of Gondwana during the Jurassic (Kopsen & McGann, 1985). Northwest extension between Australia and Greater India commenced during the Early Jurassic, creating a series of embryonic rift basins (Romine *et al.*, 1997). The Barrow Sub-basin subsided rapidly and accumulated deltaic to marine sediments in the deepest parts. This was followed by extensive, thick, marine siltstones, claystones and shales of the Dingo Claystone (Baillie & Jacobson, 1997). The onset of seafloor spreading in the Argo Abyssal Plain in the Middle to Late Jurassic was accompanied by uplift and erosion, forming the regionally recognised Callovian Unconformity (or Main Break-up Unconformity) (Romine *et al.*, 1997). Extensive submarine fan systems of the Biggada Formation, sourced from the uplifted platforms bounding the drowned rift system, were deposited at this time, punctuating the fine-grained facies of the Dingo Claystone (Kopsen & McGann, 1985; Baillie & Jacobson, 1997). The Dingo Claystone grades upward into sandstones of the Late Jurassic Dupuy Formation (Figure 6.4), deposited as marine shelf sandstones on the eastern platform and possibly as turbidite sandstones to the west and northwest on the continental slope and into the basin centre (Kirk, 1985).

Thermal subsidence continued until a period of uplift in the Late Tithonian formed the regional Base Cretaceous Unconformity (Romine *et al.*, 1997). The uplift coincided with a switch from northwest seafloor spreading in the Argo Abyssal Plain to west-northwest extension in the Gascoyne/Cuvier area. This extension was oblique to pre-existing Proterozoic and Palaeozoic fractures and resulted in the en echelon configuration of the developing Exmouth, Barrow, Dampier and Beagle Sub-basin depocentres (Romine *et al.*, 1997). The regional uplift to the south of the northern Carnarvon Basin provided the sediment source for the extensive northward-prograding Barrow Group delta-shelf complex in

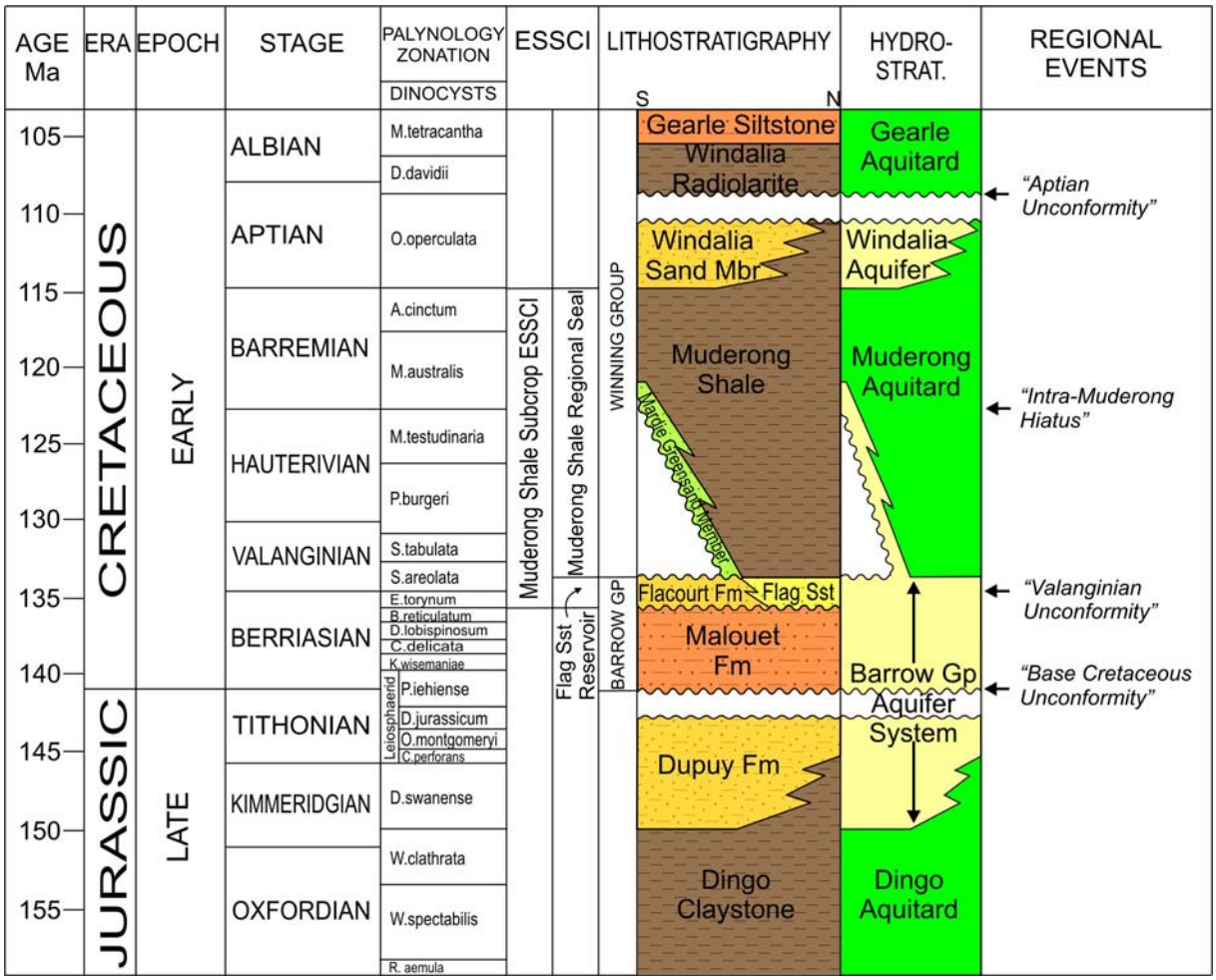

Figure 6.4 Stratigraphic column for part of the Cretaceous succession in the Barrow Sub-basin (modified after Kopsen & McGann, 1985; Shafik *et al.*, 1998; Hennig *et al.*, 2002). The location of the Muderong Shale Subcrop ESSCI in relation to the lithostratigraphic units is indicated.

the Early Cretaceous (Baillie & Jacobson, 1997; Romine *et al.*, 1997). The Barrow Group comprises 'bottomsets' of deepwater basinal shales and submarine fans of the Malouet Formation overlain by continental slope (foresets) and shoreface to wave-dominated deltaic sediments (topsets) of the Flacourt Formation (Figure 6.4). The delta-shelf margin complex prograded from the south to as far north as Barrow Island (Kopsen & McGann, 1985; Tait, 1985). Extensive submarine fan sandstones of the Flag Sandstone were deposited northward of the advancing Barrow Group delta-shelf complex in the Harriet-Campbell-Wonnich area to the north of Barrow Island (Kopsen & McGann, 1985; Osborne & Howell, 1987).

Rifting ceased in the Late Valanginian and a mature, passive margin, sag depocentre developed, accompanied by rising sea level and transgression (Kopsen & McGann, 1985; Romine *et al.*, 1997). Basal transgressive, glauconitic, marine sandstones of the Birdrong Sandstone and the Mardie Greensand Member were developed fringing the Barrow Group

delta-shelf complex and the Peedamullah Shelf, onlapping as sea level rose up the palaeoslope and shelf. The basal transgressive sandstones grade upwards into extensive, thick, deeper water marine shales of the Muderong Shale (Figure 6.4), which were deposited over the whole of the basin as transgression continued (Wiseman, 1979; Kirk, 1985; Boote & Kirk, 1989). The transgression was interrupted by a regressive regional event in the Early Barremian, leading to the development of the Intra-Muderong Hiatus, represented by an angular unconformity in the deeper basin area around the Montebello Islands (Kirk, 1985; Romine *et al.*, 1997). Maximum transgression occurred during the Middle to Late Barremian (*M. australis* or *A. cinctum* palynology zone) whilst the Muderong Shale was still being deposited, coincident with the highest rates of tectonic subsidence (Romine *et al.*, 1997).

The overall transgressive pattern continued until the Turonian, although was interrupted locally in the Aptian with the deposition of fine-grained, below storm wave-base, shallow marine sandstones of the Windalia Sandstone Member (Figure 6.4) (Campbell *et al.*, 1984; Kopsen & McGann, 1985). In the Late Cretaceous, the fine-grained, pelagic siliciclastic sediments were gradually replaced by calcareous pelagic sediments along the whole of the North West Shelf and the Tertiary was characterised by widespread, dominantly carbonate progadation (Kopsen & McGann, 1985; Romine *et al.*, 1997). Collision and underthrusting of the Australian Plate beneath the Southeast Asian Plate in the Late Miocene caused some reactivation of older structures and tightening of folds (Boote & Kirk, 1989; Baillie & Jacobson, 1997).

6.2.2 Pressure, Temperature and Salinity Conditions

The phase state of CO_2 when injected into the subsurface is dependent on the *in situ* pressure and temperature conditions, thus it is necessary to define the pore fluid pressure and geothermal gradients of the basin. Temperature gradients in the Barrow Sub-basin range from 29.98ºC/km at Sinbad-1 to 38.73ºC/km at Agincourt-1 ST1. The average temperature gradient is 34.27ºC/km (Figure 6.5 and Appendix C). The average hydrostatic pore fluid pressure gradient in the Barrow Sub-basin is 9.8 MPa/km (Figure 6.5 and Appendix B). Based on these gradients, the depth for CO_2 to be in the supercritical phase is about 750 m. The Flag Sandstone and Mardie Greensand Member reservoirs are deeper than 750 m in the area of interest (the shallowest depth of the Mardie Greensand Member is 845 m at Barrow Deep-1), so injected CO_2 will remain in the supercritical phase. Salinity varies from 23000 ppm at Bambra-2 to 94000 ppm at Cycad-1. The average salinity is 32189 ppm.

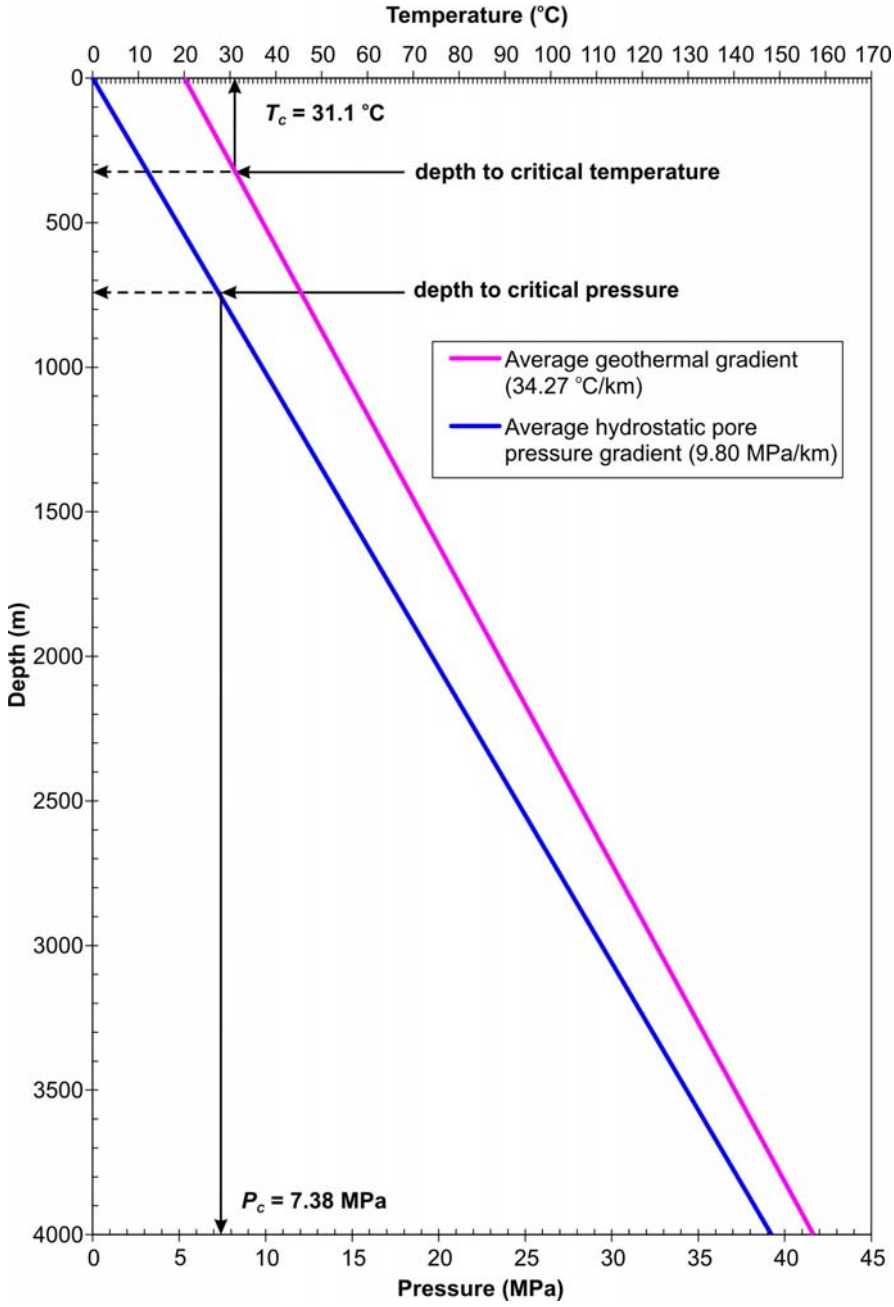

Figure 6.5 Depth to CO_2 critical temperature (T_c) and critical pressure (P_c) in the Barrow Sub-basin.

6.3 METHODOLOGY FOR DETAILED SITE CHARACTERISATION

The methodology for detailed site characterisation was discussed in a previous chapter. A brief summary is provided here, focussing on the geological characterisation aspects that were undertaken for this PhD study (Figure 6.6). Seismic structural and stratigraphic interpretations were integrated with wireline log well correlations, detailed sedimentological core descriptions and biostratigraphy, to develop structural and stratigraphic models for the

potential site. These models provided the subsurface framework and formed the basis for the assessment of three principle aspects: injectivity, containment and capacity.

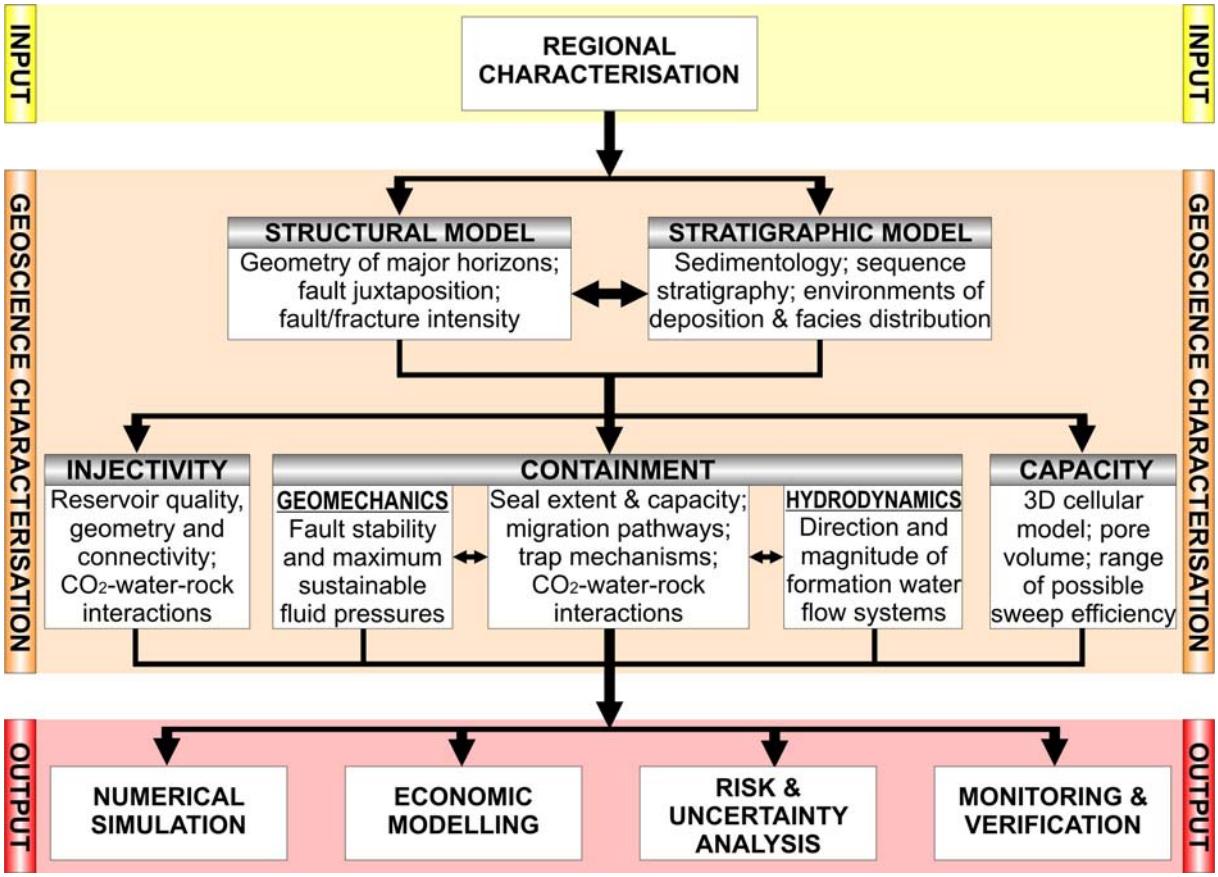

Figure 6.6 Workflow followed to geologically characterise potential sites for geological storage of CO_2.

Factors that influence injectivity include the geometry and connectivity of individual flow units, the nature of the heterogeneity within those units (i.e. the likely distribution and impact of baffles such as interbedded siltstones and shales) and the physical quality of the reservoir in terms of porosity and permeability characteristics (Figure 6.6). The sedimentary depositional models derived from the sequence stratigraphic interpretation provided information about the reservoir distribution and the likely lateral and vertical connectivity, as the geometry and spatial distribution of individual flow units is a function of their environment of deposition. The reservoir quality was assessed via detailed analysis of core plug porosity and permeability characteristics, petrography and wireline log petrophysical interpretation. The petrographic study was undertaken by Kraishan *et al*. (2003) and the petrophysics interpretation was provided by Skinner (2001) and O'Sullivan (2003), the key results of which were integrated into this study.

Factors relating to containment include the distribution and continuity of the seal, the seal capacity (maximum CO_2 column height retention), potential migration pathways (structural geometry, distribution and extent of intraformational seals, and formation water flow direction and rate) and the integrity of the reservoir and seal (fault/fracture stability and maximum sustainable pore fluid pressures) (Figure 6.6). Collected core samples were subjected to mercury injection capillary pressure (MICP) analysis to evaluate the CO_2 retention capacity of the rocks. Geomechanical studies by Streit (2003) used *in situ* stress and rock strength data to determine maximum sustainable pore pressure increases, the results of which were integrated into this study to assess the reactivation risk of faults in the area. The past and present formation water flow systems were characterised by Hennig *et al*. (2003) from pressure-elevation plots and hydraulic head distribution maps, and integrated into this study to interpret the possible impact on CO_2 migration and containment.

Potential CO_2 storage capacity was assessed geologically in terms of available pore volume; however, the efficiency of that storage capacity will be dependent on the rate of CO_2 migration, the potential for fill-to-spill structural closures encountered along the migration path, and the long-term prospects of residual trapping, dissolution into the formation water or precipitation into new carbonate minerals (Figure 6.6). The pore volume was estimated using the calculation method described in Chapter 3.

6.4 STRUCTURAL MODEL

The structural model defines the gross geometry of the reservoir and seal units and identifies structural features such as faults and their juxtaposition relationships. The structural framework is critical to understanding and predicting how injected CO_2 will migrate within the subsurface over the long-term. The structural framework of the Barrow Sub-basin was constructed using the seismic interpretation (where the data was of sufficient coverage), well correlation and previously published structure maps.

6.4.1 Structural Geometry

The structural geometry in the study area of the Barrow Sub-basin is quite complex. A depth structure map of the base Muderong Shale (base regional seal) was created by an amalgamation of seismic interpretation (over the Harriet-Campbell area), interpreted stratigraphic well markers and previously published structure maps of Campbell *et al*. (1984) and Kopsen and McGann (1985) (Figure 6.7).

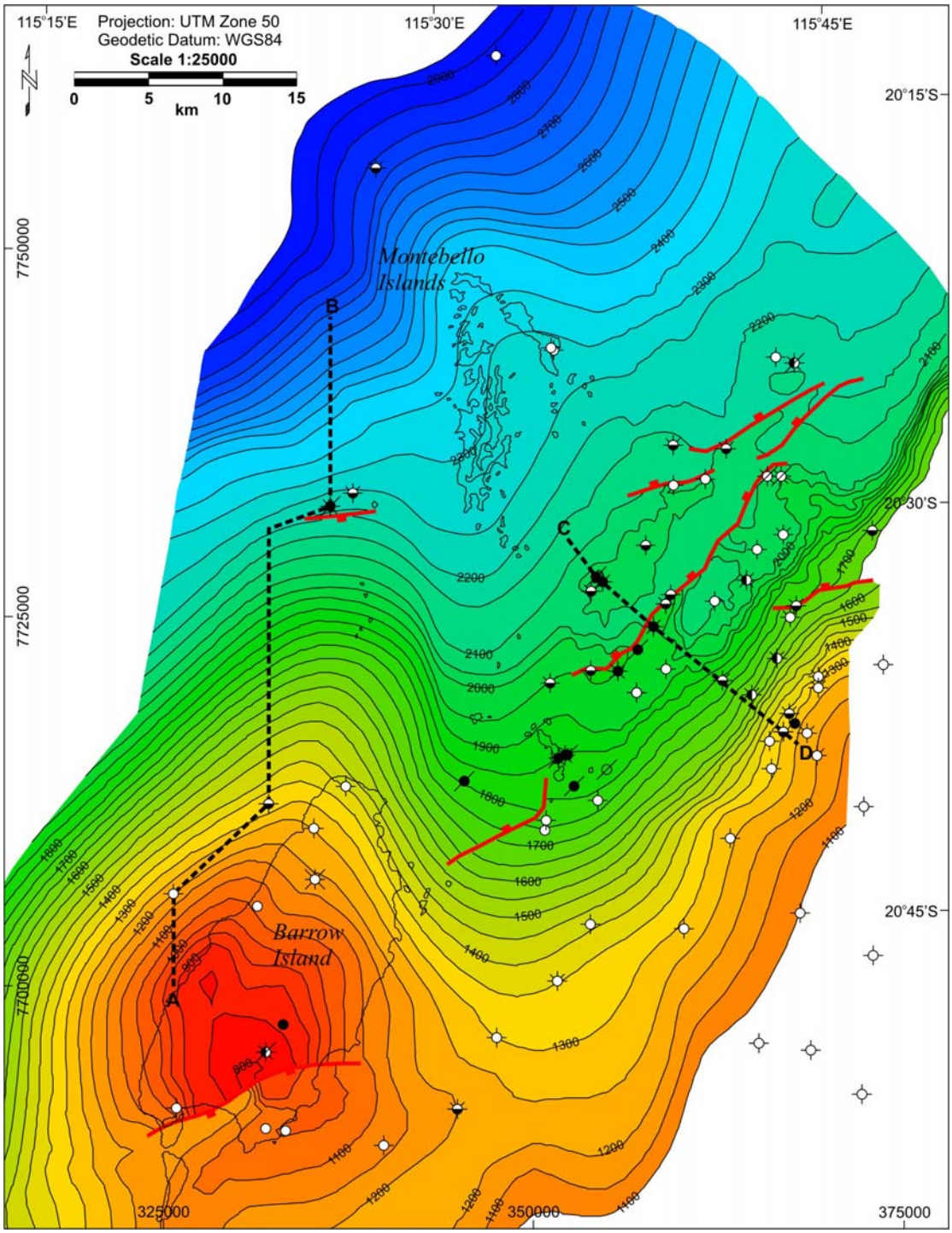

Figure 6.7 Depth structure map of the Base Muderong Shale surface.

The surface is deepest in the northwest and shallows southward towards a high at Barrow Island and southeastward towards the Peedamullah Shelf. The high at Barrow Island is formed by a large, fault-bound, northward-plunging anticline. This structural feature continues higher up into the sedimentary succession and is the same structure that traps the oil of the overlying Barrow Island oil field accumulation. A smaller fault-bound structural

closure at the nose of the plunging anticline provides the structural trap for the Wonnich gas field. On the eastern side of the study area are some low relief, four-way dip closed anticlines, which provide the traps for the Bambra, Campbell and Ulidia gas fields. In addition, there are a series of large, northeast-southwest trending faults (downthrown to the northwest), which provide fault-bound structural closure traps for oil and gas accumulations such as the Harriet oil field and Sinbad gas field. Beyond the large faults of the Harriet-Campbell area, the surface continues to dip up toward the southeast margin of the basin, onlapping onto the flanks of the Peedamullah Shelf with no further structural closures (the oil and gas accumulations of the Gipsy-Rose-Lee fields are trapped deeper in underlying Jurassic structures). Figure 6.8 shows an interpreted seismic line through the Barrow Island anticline (NW Barrow 3D Survey) and Figure 6.9 shows an interpreted seismic line through the Harriet-Campbell area towards the Peedamullah Shelf (Cash 3D Survey), highlighting the different structural geometries toward the south and southeast.

The two distinct structural trends mean that there are two specific potential CO_2 injection site locations that can be considered. This is confirmed by plotting flow vectors indicating the direction of maximum upward dip onto the Base Muderong Shale depth structure surface (Figure 6.10). Analysis of this map clearly indicates two main potential CO_2 migration directions based on the structural trends: south towards Barrow Island or southeast towards the Peedamullah Shelf. For the purposes of this study, it was decided to focus the geological model on the southward trend over Barrow Island, for the following reasons:

1. Both directions would encounter existing hydrocarbon accumulations up-dip. However, the Barrow Island oil field is a mature, depleted field in a stratigraphically shallower interval, whereas the Harriet-Campbell fields are more recent production developments within the same stratigraphic interval as the CO_2 injection horizon. Therefore, the Barrow Island trend has less likelihood of potentially compromising an existing resource whilst it is still being actively produced.
2. Future hydrocarbon exploration potential that could be compromised by CO_2 injection is also much less likely in the Barrow Island area due to the maturity of exploration and development, whilst there is still some considerable potential for continued exploration in the Harriet-Campbell area.

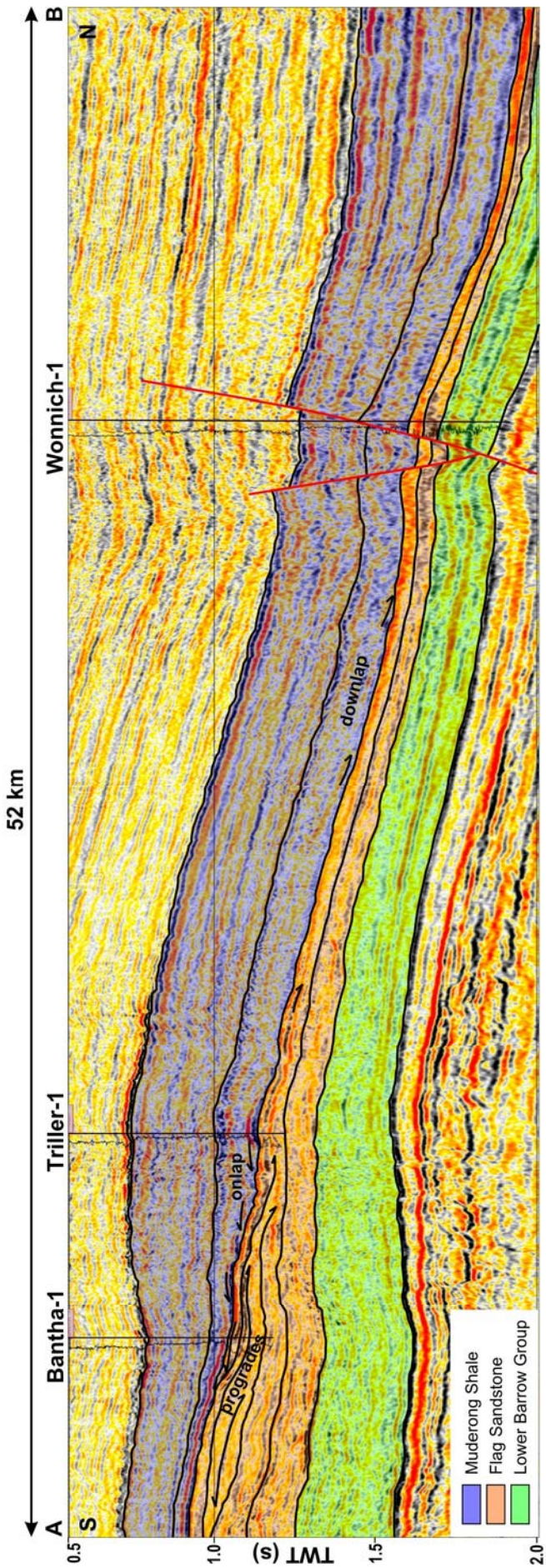

Figure 6.8 Seismic interpretation of A - B regional seismic line through the NW Barrow 3D seismic survey (the location of the section is shown on Figure 6.7).

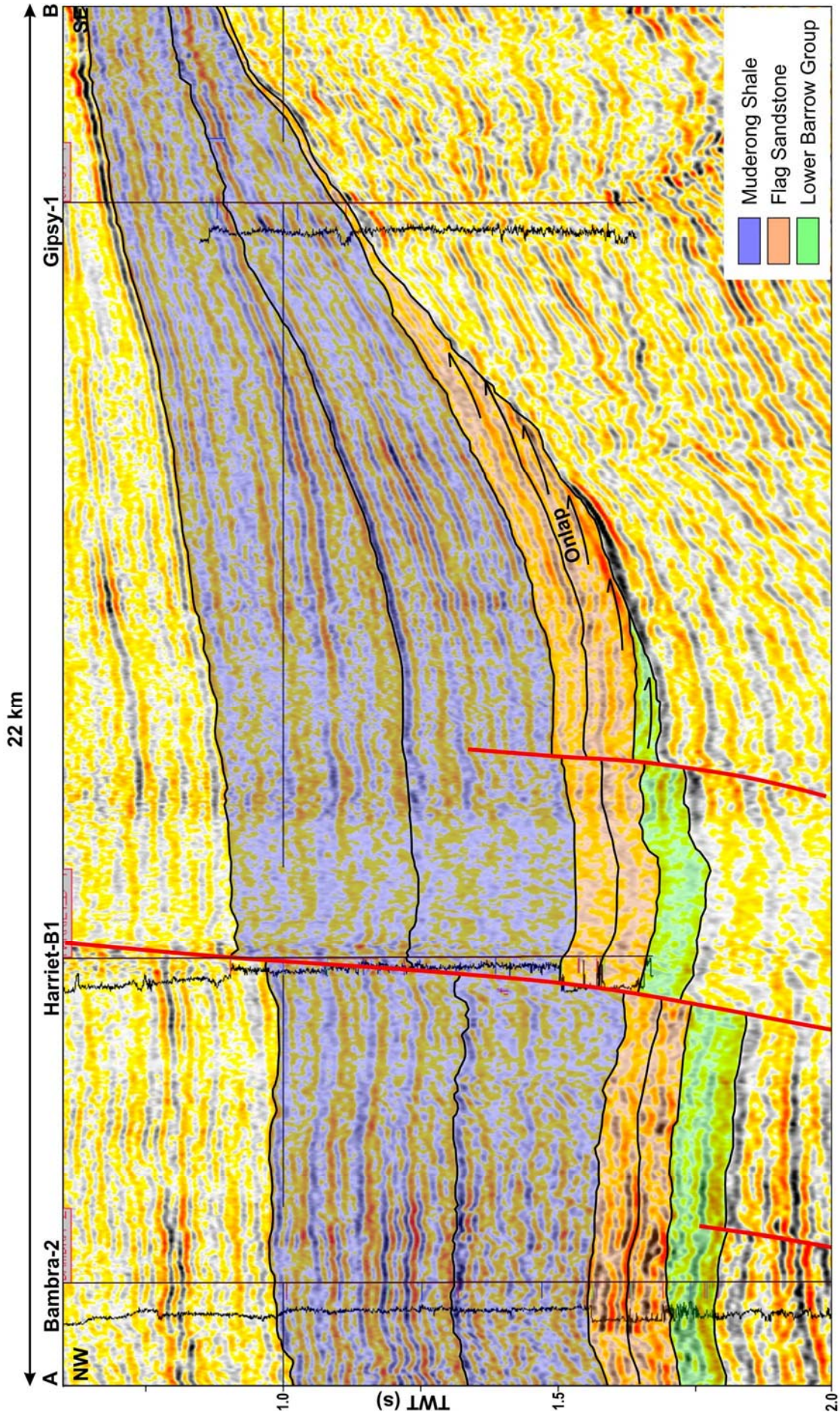

Figure 6.9 Seismic interpretation of C - D regional seismic line through the Cash 3D seismic survey (the location of the section is shown on Figure 6.7).

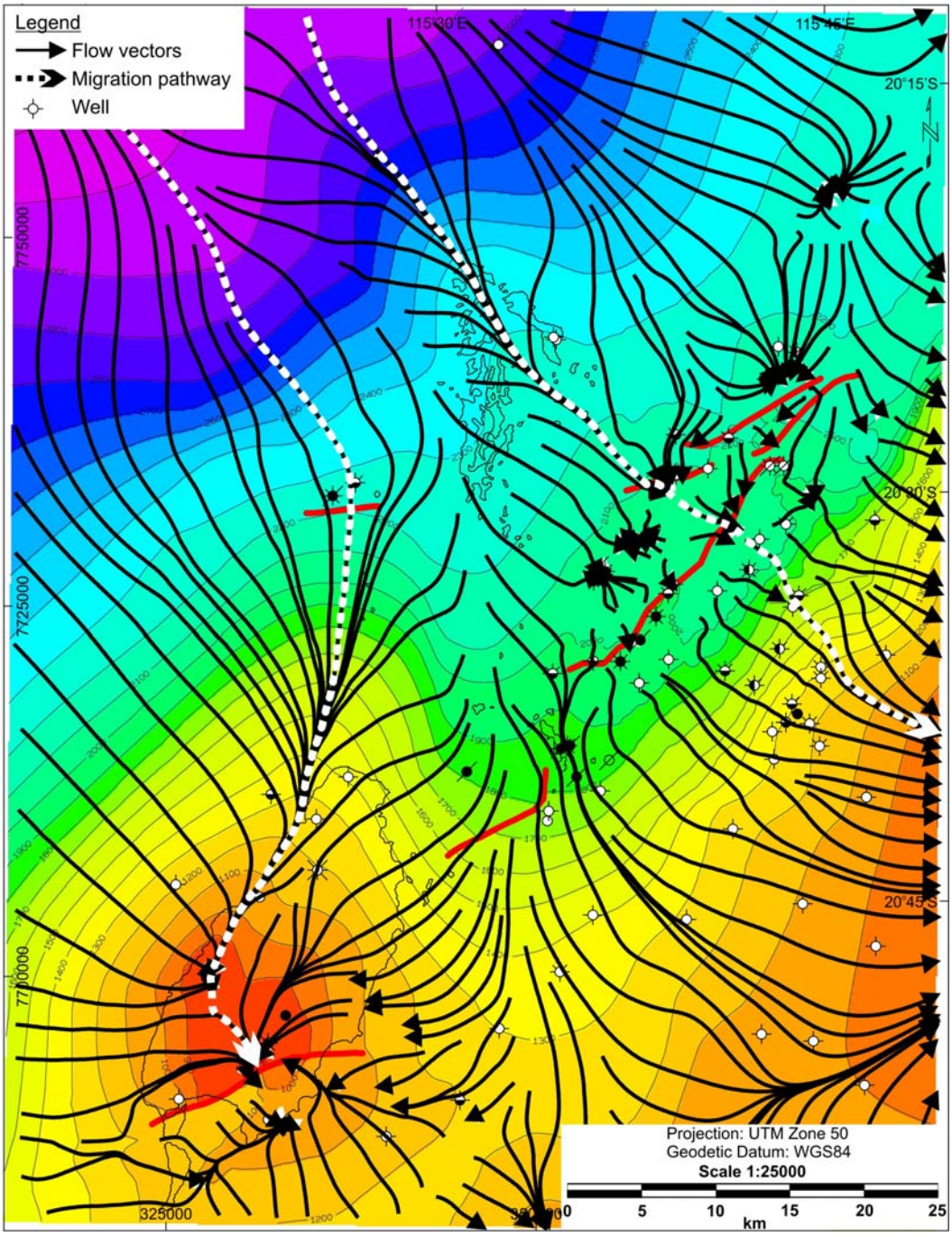

Figure 6.10 Potential CO_2 migration pathways based on the structural geometry of the Base Muderong Shale (base regional seal) depth structure surface.

3. The Barrow Island trend is much simpler structurally, as it consists of a single anticline axis uninterrupted by faults over a distance of approximately 40 km between the Wonnich and Barrow Island faults. The Harriet-Campbell area, in comparison, has smaller, low relief anticlinal closures, numerous large-scale faults within the migration pathway, and no defined structural closure beyond the faults of the Harriet-Campbell area.

4. The fault juxtaposition relationships are more favourable for containment along the Barrow Island trend, as the Flag Sandstone/Flacourt Formation is upthrown against the Muderong Shale. In the Harriet-Campbell area in the direction of potential CO_2 migration, the Flag Sandstone is downthrown against Lower Barrow Group sediments, so there is a higher potential for cross-fault migration.
5. The fault-bound anticline at Barrow Island provides a physical trap for any free-phase CO_2 that is not trapped by other mechanisms along the migration pathway (subject to the sealing quality of the Barrow Island fault). The Harriet-Campbell trend provides no up-dip structural closure beyond the existing oil and gas fields and the migration pathway length may not be long enough to ensure that CO_2 is trapped by other mechanisms, such as residual or solubility trapping.
6. Potential storage capacity may be greater within the Barrow Island trend as the reservoir thickens towards Barrow Island. The Flag Sandstone in the Harriet-Campbell area, in comparison, thins towards the basin margin as it onlaps onto the Peedamullah Shelf.
7. There is greater confidence that the Muderong Shale continues to be an effective seal in a southward direction, as south of Barrow Island along the same anticlinal trend the South Pepper field is sealed by the Muderong Shale. However, there are no hydrocarbon accumulations beneath the Muderong Shale southeast of the Harriet-Campbell fields, so the continued competency of the Muderong Shale in that area is unknown.

Depth structure surfaces of the key reservoir and seal bounding horizons for the Barrow Island structural trend are shown in Figure 6.11, Figure 6.12 and Figure 6.13. The structural geometry of all the horizons is very similar, with all surfaces clearly showing the northward-plunging fault-bound anticline. The depth of the Top Flag Sandstone does not get shallower than about 850 m, therefore the injected CO_2 is likely to remain in the supercritical phase.

6.4.2 Fault Characteristics

There are several large-scale normal faults within the study area of the Barrow Sub-basin, penetrating through the entire reservoir and overlying regional seal (Figure 6.14). These play an important role in the distribution of hydrocarbons, and several oil and gas fields are located in fault-dependent structural traps (e.g. Barrow Island, Harriet, Sinbad, Wonnich). Within the Barrow Island trend area, two major normal faults intersect the anticlinal structure: the

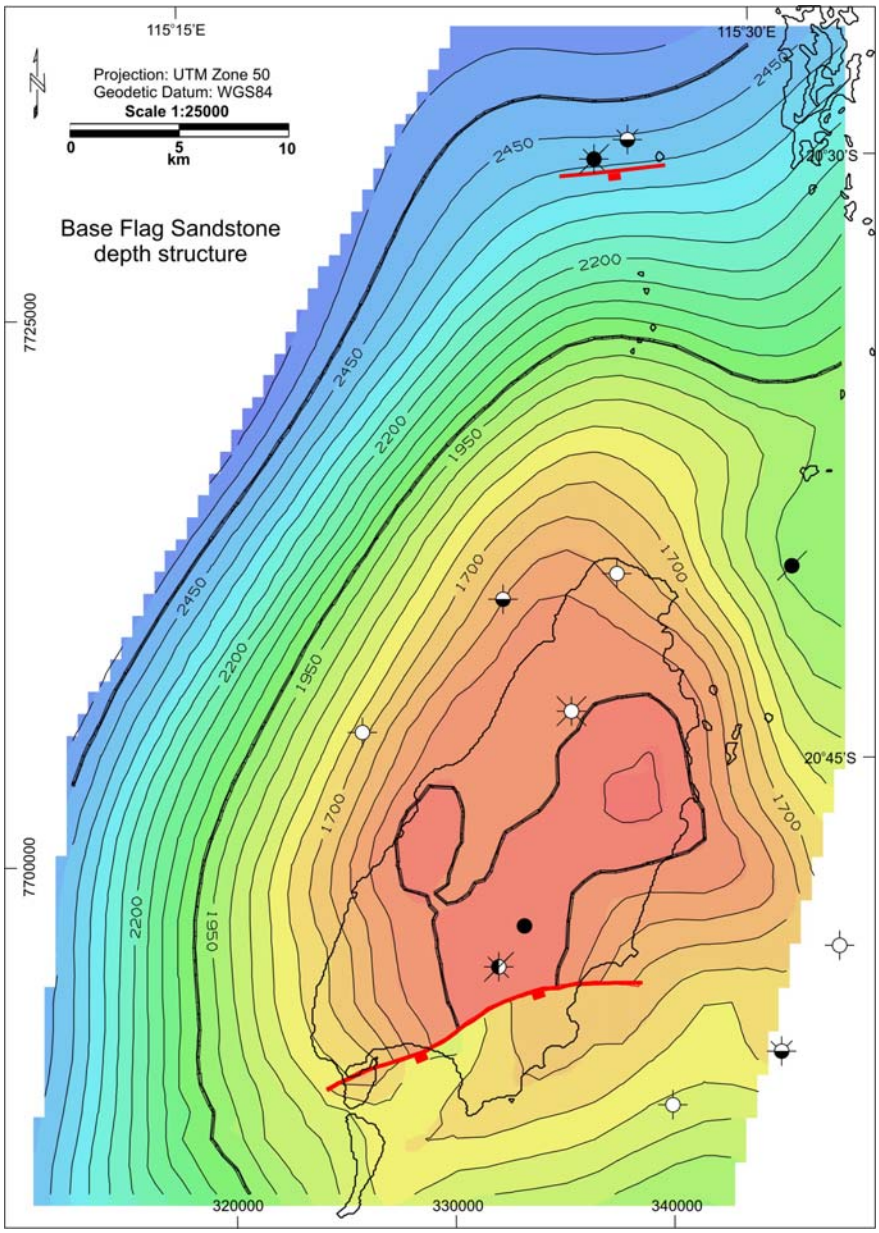

Figure 6.11 Depth structure map of Base Flag Sandstone surface.

Wonnich Fault on the south side of the Wonnich gas field and the Barrow Island Fault at the southern end of Barrow Island. In the Harriet-Campbell area there are at least four major normal faults that penetrate through the Cretaceous succession. The orientation and dip of some of the faults within the study area are detailed in Table 6.1. The faults in the Barrow Island trend area strike in an east-northeast direction and are downthrown to the south, whereas the faults in the Harriet-Campbell area strike in a northeast direction and are downthrown to the northwest. The dips of the faults vary from 36° to 69°.

The large-scale normal faults identified within the study area may pose a potential risk to CO_2 containment, especially as the faults penetrate all the way through the reservoir and the

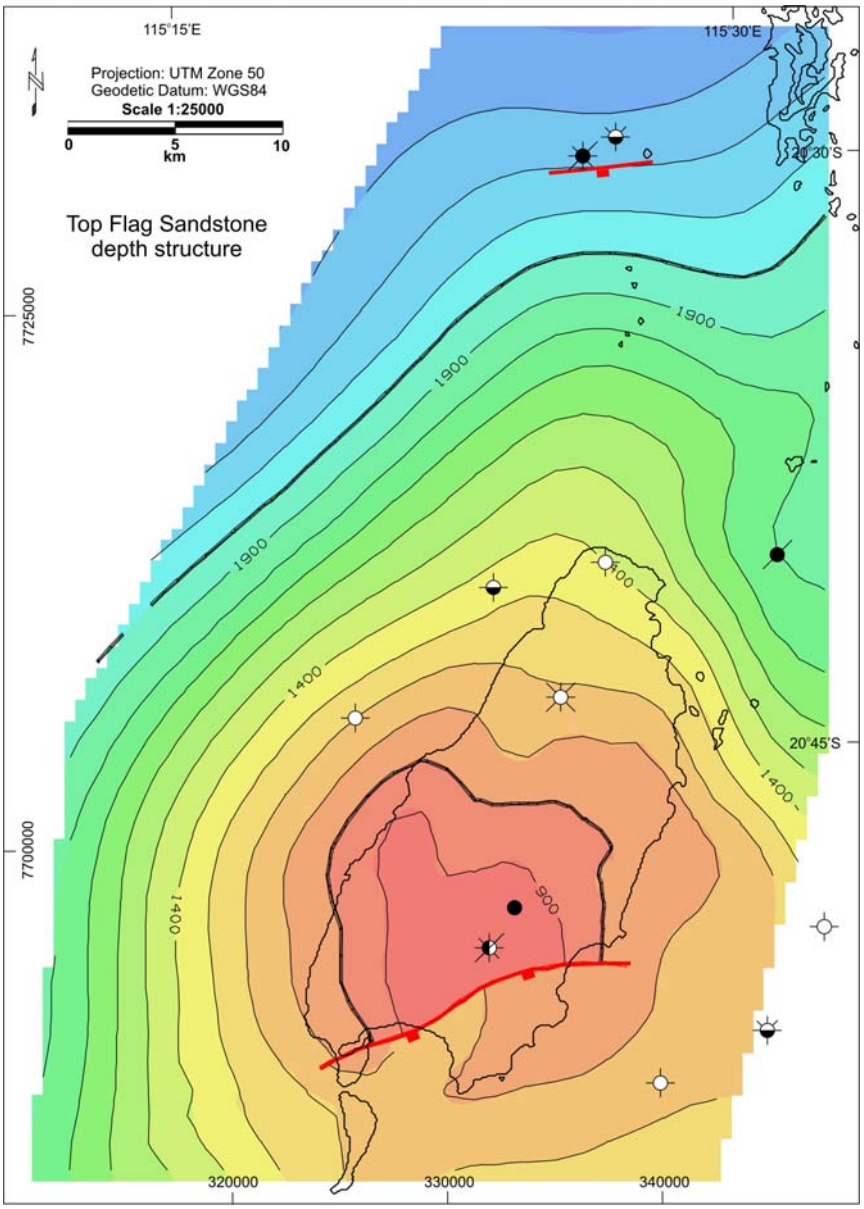

Figure 6.12 Depth structure map of Top Flag Sandstone surface.

overlying seal. However, the presence of fault-dependent hydrocarbon accumulations in the same area provides confidence that the faults are currently sealing and are capable of retaining hydrocarbon columns (both oil and gas). Subsurface injection of CO_2 may potentially reactivate pre-existing faults, depending on the prevailing *in situ* stresses and pressures. The geomechanical stability of the faults and the potential for CO_2 containment breach is discussed later in section 6.7.4.

Small-scale faults are also imaged on seismic sections, distorting high amplitude seismic reflectors within the Muderong Shale regional seal (Figure 6.15). They occur immediately beneath the intra-Muderong hiatus and appear to only extend downwards for 50–70 ms

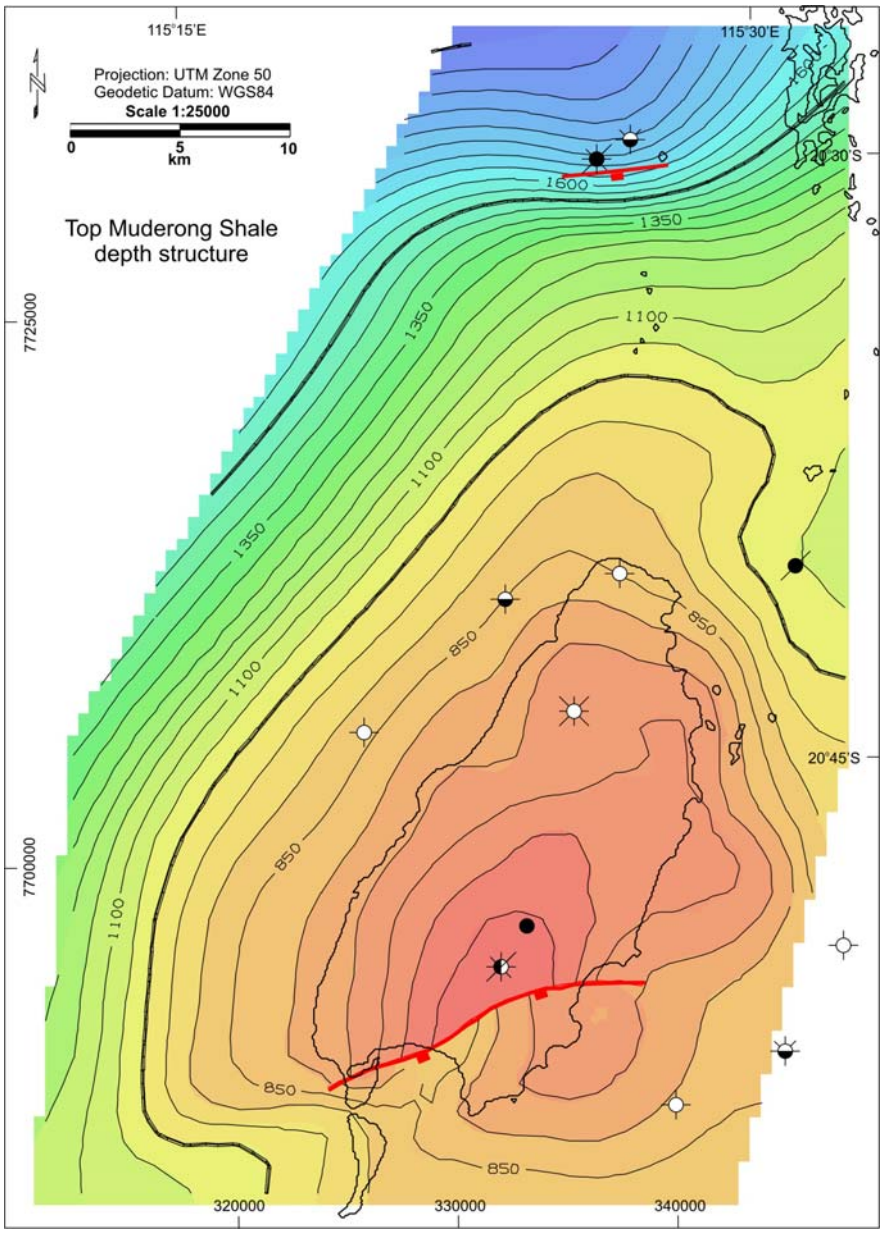

Figure 6.13 Depth structure map of Top Muderong Shale surface.

two-way time, but may actually extend to the base of the Muderong Shale (indistinct seismic quality in this interval). When viewed as a horizontal time-slice (Figure 6.15), these faults appear to connect in polygonal shapes, which can be likened in appearance to sedimentary mud-cracks. The exact cause of polygonal fault systems like these is a matter of some debate. One interpretation is that the fine-grained sediments have shrunk due to syneresis (spontaneous volumetric contraction with concurrent pore fluid expulsion) (Dewhurst *et al.*, 1999). Alternatively, the creation of polygonal fault systems may result from shear failure due to a low coefficient of friction in the fine-grained sediments (Goulty, 2001). The impact of this polygonal fault system on the potential sealing capabilities of the Muderong Shale is

Table 6.1 Geometry of key faults in the Barrow Sub-basin study area.

Fault Name	Location	Depth (m) †	Average Strike Direction	Dip Angle	Dip Direction	Down-throw (m)	Source
Barrow Fault	Barrow Island	800	045ºN–060ºN	69º	SE	180	Kloss (1996)
Lowendal Fault	Bambra	1950	045ºN	65º	NW	100	Kloss (1996)
Lowendal Fault	Harriet	1900	045ºN	49º	NW	100	Kloss (1996)
Lowendal Fault	Sinbad	2000	020º–060ºN	53º	NW	65	Kloss (1996)
Main Fault	Tanami	1850	010º–045ºN	51º	NW	20	Kloss (1996)
Orpheus Fault	Campbell	2200	060ºN	36º	NW	40	Kloss (1996)
Wonnich Fault	Wonnich	2300	080ºN	48º	S	≈ 60	This study

† Indicates the approximate depth at which the fault dip has been estimated.

unclear at present; however, the large number of successful hydrocarbon accumulations beneath the Muderong Shale suggests that they have limited impact on the effectiveness of the seal.

6.5 STRATIGRAPHIC MODEL

The stratigraphic model determines the sedimentary environments of deposition and likely facies distribution, both laterally and vertically. The stratigraphic framework is important for understanding the distribution of reservoir properties (such as porosity and permeability), which are critical to the ease with which CO_2 can be injected, how it might disperse and the volume that can be stored. The stratigraphy of the Barrow Sub-basin was evaluated through the sedimentology, well correlation, seismic facies and sequence stratigraphic interpretation.

6.5.1 Sedimentology

Numerous sedimentary cores were viewed for this study; however, the majority of the data came from the wells in the Harriet-Campbell area rather than the Barrow Island trend. Fortunately, though, there was a considerable amount of core data from Wonnich-1, which is the closest well to the likely CO_2 injection point. A total of 27 lithofacies were identified from within the cored intervals, based on variations in characteristics such as colour, bedding, composition, texture, fossils and sedimentary structures. The various lithofacies are shown in

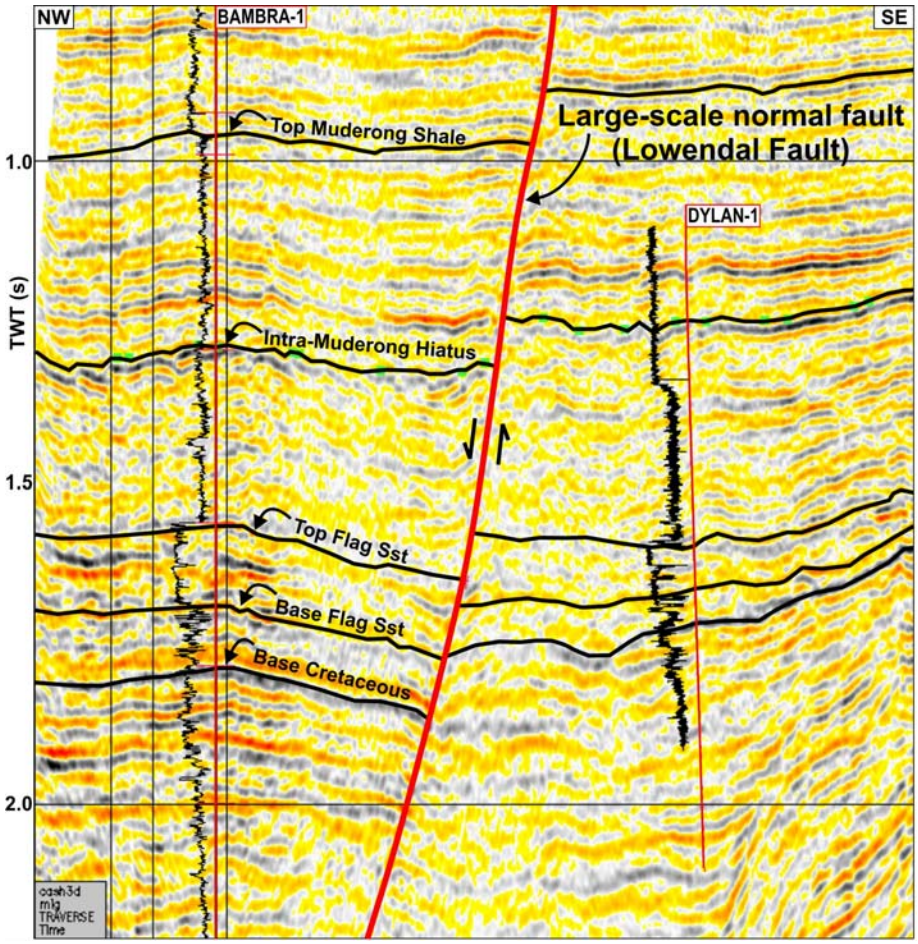

Figure 6.14 Example of large-scale faulting in the Barrow Sub-basin (seismic line through Cash 3D seismic survey). The fault imaged here is the Lowendal Fault in the Harriet-Campbell area.

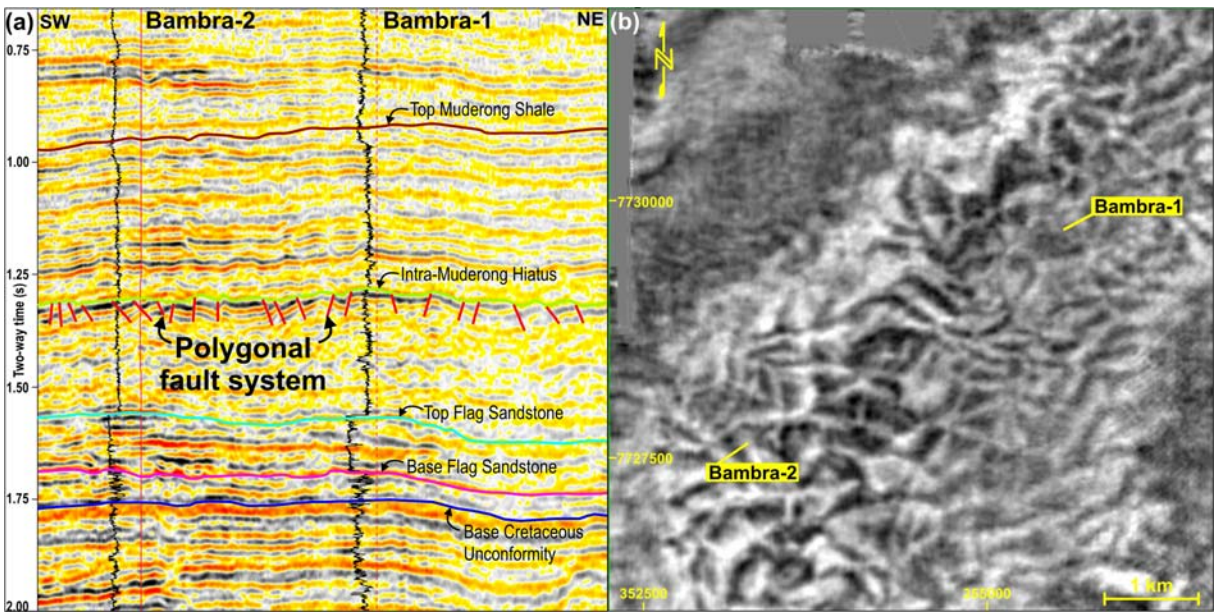

Figure 6.15 Vertical and horizontal seismic images of the polygonal fault system beneath the intra-Muderong hiatus within the Muderong Shale regional seal. (a) Approximate southwest-northeast cross-section through the Cash 3D seismic survey at the Bambra Field location. (b) Horizontal time-slice (unflattened) at 1328 ms through the Cash 3D seismic survey over the Bambra Field area.

Figure 6.16 and described in Table 6.2. The lithofacies were grouped together into facies associations and an interpretation made as to their possible depositional environment. Four facies associations were identified in total and are described below (Table 6.2).

6.5.1.1 Facies Association A – Mid to Outer Shelf

Facies Association A comprises lithofacies 1 to 7, and is representative of the Mardie Greensand Member and the eastern margin and upper Muderong Shale. The clay, silt and very fine sand grain sizes indicate a low energy depositional environment. The presence of medium-grained sandstones grading into the finer-grained sediments suggests occasional higher energy depositional pulses. The intensity of the bioturbation and overprinting of any primary sedimentary structures that may have existed indicates that the sedimentation rate was quite slow, to allow for complete biogenic reworking. The presence of glauconite and occasional shell fragments indicate that the rocks were most likely deposited within a marine environment. Therefore, the probable environment of deposition was on the mid to outer marine shelf.

6.5.1.2 Facies Association B – Proximal to Mid Basin Floor Fan

Facies Association B comprises lithofacies 8 to 18, and is representative of the Flag Sandstone. The most common lithofacies within this association are the massive sandstones. These are very thick-bedded, monotonous sandstones, typically 1-3 m thick but can be up to 20 m thick, with no observable sedimentary features. The relatively coarse grain size, poor sorting and lack of mud matrix material indicate that the sediments were deposited within a high energy depositional environment. A lack of sedimentary features such as-cross bedding suggest that the sediments were not deposited by traction currents. The most likely mode of deposition is by high density mass flows, such as sandy debris flows or high-density turbidity currents. This interpretation is supported by the sedimentary structures that have been observed in the associated fine- to medium-grained sandstones. These include erosional bases to the sandstone beds and mudstone rip-up clasts caused by erosional scouring of successive mass flows, dish and pillar structures formed as a result of water escape and sediment dewatering, plus evidence of slumping due to sediment instability. These features and the close linkage with Facies Associations C and D (described below; Facies Association B typically grades into Facies Association C) lead to the interpretation that the sediments are deep water basin floor fans. Facies Association B sediments were deposited by sandy debris

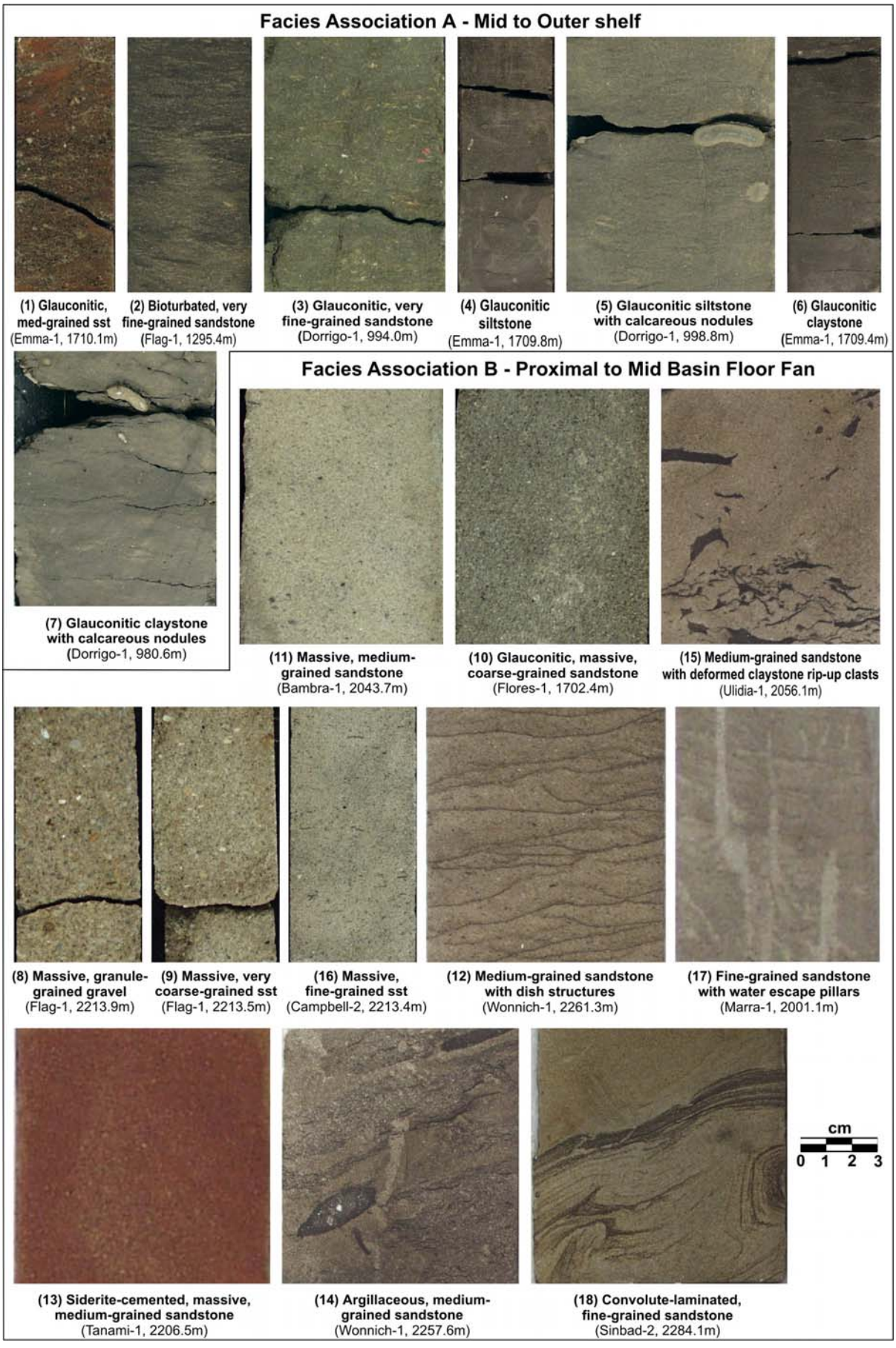

Figure 6.16 Core photographs of lithofacies and their interpreted facies associations.

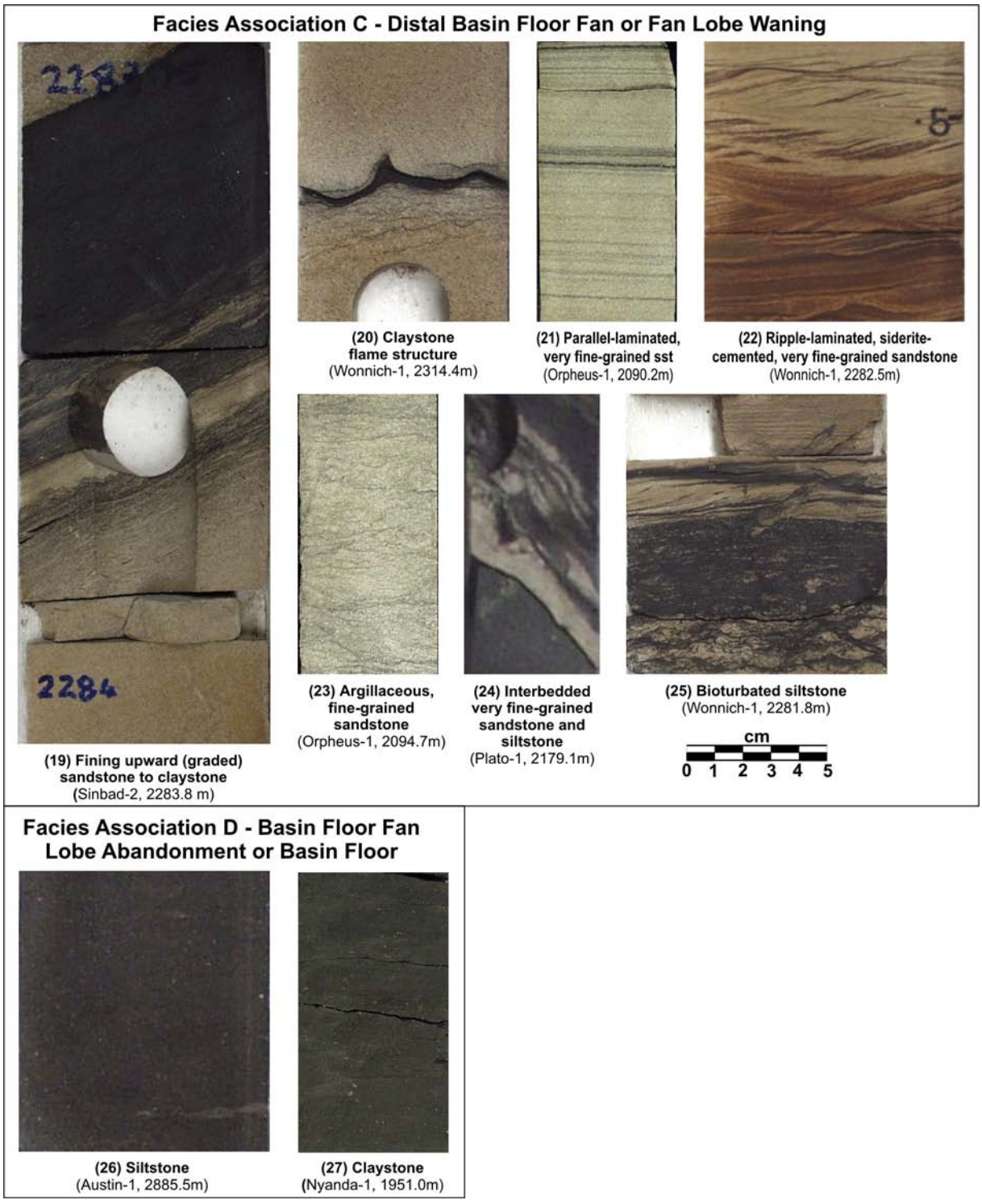

Figure 6.16 Core photographs of lithofacies and their interpreted facies associations.

Table 6.2 Sedimentary core lithofacies, facies associations and interpreted depositional environments.

Fm	No	Name	Lithofacies Description	Facies Association – Interpretation	
MARDIE GREENSAND / MUDERONG SHALE	1	Glauconitic, medium-grained sandstone	Green-grey to orange, predominantly medium-grained argillaceous sandstone. Sorting is poor (ranging from very coarse to fine) and grains are sub-angular to sub-rounded. Sandstone is well to very well consolidated, especially where siderite-cemented. Common glauconite and high mud matrix content with abundant wavy mud laminae. Extensive bioturbation, which has overprinted any primary structures. Rare granule-sized clasts of glauconite & quartz are also present.	FACIES ASSOCIATION A	Mid to outer shelf
	2	Bioturbated, very fine-grained sandstone	Olive green-grey to brown-grey, very fine-grained argillaceous sandstone. Framework grains are sub-rounded and well sorted, composed predominantly of quartz plus minor glauconite. Sandstone is well consolidated and siderite-cemented in parts. Abundant wavy mud laminae are present, which have been disturbed by intense bioturbation. Bioturbation over-prints primary structure; however, thinly interbedded layers of very fine-grained sandstone and siltstone are resolvable. Burrows are sub-horizontal to inclined.		
	3	Glauconitic, very fine-grained sandstone	Olive green, very fine-grained argillaceous sandstone. Abundant wavy mud laminae and extensive bioturbation, with some burrows siderite-cemented.		
	4	Glauconitic siltstone	Green-grey, argillaceous siltstone. Abundant wavy mud laminae and bioturbation. Rare to common floating coarse grains of quartz and glauconite present.		
	5	Glauconitic siltstone with calcareous nodules	Olive green-grey, argillaceous siltstone. Abundant wavy mud laminae and bioturbation. Occasional siderite-cemented burrow. Rare to common calcareous nodules (typically 1–2 cm, but occasionally very large, up to 30 cm).		

Fm	No	Name	Lithofacies Description	Facies Association – Interpretation	
MARDIE GREENSD / MUDERONG	6	Glauconitic claystone	Dark grey claystone. Texture is typically hard and blocky, with some fissility. Occasional very thin interbeds/lenses of siltstone/very fine-grained sandstone are present. Also contains rare to common floating coarse grains of quartz and glauconite.	FACIES ASSOCIATION A	Mid to outer shelf
	7	Glauconitic claystone with calcareous nodules	Olive green-grey, glauconitic claystone, varying from slightly fissile to very fissile. Rare to common calcareous nodules (typically 1–2 cm, but occasionally very large, up to 15 cm). Occasional shell fragments & siderite nodules are also present.		
FLAG SANDSTONE	8	Massive, granule-grained gravel	Massive (structureless), light brown-grey, granule-sized gravel. Grains are sub-angular and poorly sorted (predominantly granule, but ranging from pebble to fine). Composed of mainly quartz, plus minor lithics and other minerals (feldspar?).	FACIES ASSOCIATION B	Proximal to mid basin floor fan
	9	Massive, coarse- to very coarse-grained sandstone	Massive (structureless), light grey, coarse to very coarse-grained sandstone. Grains are sub-angular and poorly sorted (predominantly coarse, but ranging from very coarse to very fine). Composed of mainly quartz, plus minor lithics and other minerals (feldspar?). Generally well consolidated. Rare to common small horizontally-orientated elongate mud clasts (tealeaf texture) also present.		
	10	Glauconitic, massive, coarse-grained sandstone	Same as Lithofacies 9 above but light green-grey in colour due to additional glauconite constituent.		
	11	Massive, medium-grained sandstone	Massive (structureless), light grey, medium-grained sandstone. Grains are sub-angular and poorly to moderately sorted (predominantly medium, but ranging from coarse to very fine). Composed of mainly quartz, plus minor lithics and other minerals (feldspar?). Generally well consolidated but sometimes poorly to moderately consolidated. Rare to common small horizontally-orientated elongate mud clasts (tealeaf texture) also present.		
	12	Medium-grained sandstone with dewatering features	Same as Lithofacies 11 above but also contains dewatering features, such as dish structures and water escape pipes.		

Fm	No	Name	Lithofacies Description	Facies Association – Interpretation	
FLAG SANDSTONE	13	Siderite-cemented, massive, fine- to medium-grained sandstone	Same as Lithofacies 11 and 16 but with siderite cement, resulting in an orange-grey colour and very well consolidated.	FACIES ASSOCIATION B	Proximal to mid basin floor fan
	14	Argillaceous, medium-grained sandstone	Light brown-grey, argillaceous, medium-grained sandstone. Grains are sub-angular and poorly sorted (predominantly medium, but ranging from coarse to very fine). Composed of mainly quartz, plus minor lithics and other minerals (feldspar?). Generally well consolidated. Abundant wavy and convoluted mud laminae. Rare to common dewatering features (such as water escape pipes) and claystone rip-up clasts.		
	15	Fine- to very coarse-grained sandstone with claystone rip-up clasts	Same as Lithofacies 9, 11 and 16 but with rare to common claystone rip-up clasts. The rip-up clasts vary in size from a few mm up to 10 cm and sometimes show evidence of soft-sediment distortion.		
	16	Massive, very fine- to fine-grained sandstone	Massive (structureless), light grey, fine- to very fine-grained sandstone. Grains are sub-angular to sub-rounded and poorly to moderately sorted (coarse to very fine). Composed of mainly quartz, plus minor lithics and other minerals (feldspar?). Generally well consolidated. Rare to common small horizontally-orientated elongate mud clasts (tealeaf texture) are also present. Rare siderite nodules.		
	17	Fine-grained sandstone with dewatering features	Same as Lithofacies 16 above but also contains dewatering features, such as dish structures and water escape pipes.		
	18	Convolute-laminated, fine-grained sandstone	Light grey, fine-grained sandstone. Moderately to well sorted with sub-angular to sub-rounded grains. Convoluted mud laminations are present.		
	19	Fining upward (graded) sandstone to claystone	Grain size varies rapidly from sandstone to claystone up-section (coarse-tail, normal grading). Typically sharp contact with overlying sandstone bed.	FACIES ASS. C	Distal basin floor fan or fan lobe waning
	20	Claystone flame structure	Dark grey claystone at the top of rapidly fining sandstone bed, formed into a flame structure and protruding into the overlying sandstone bed.		

Fm	No	Name	Lithofacies Description	Facies Association – Interpretation	
FLAG SANDSTONE	21	Laminated, very fine- to fine-grained sandstone	Light grey, very fine- to fine-grained sandstone. Moderately to well sorted with sub-angular to sub-rounded grains. Parallel, ripple or wavy mud laminations are present.	FACIES ASSOCIATION C	Distal basin floor fan or fan lobe waning
	22	Laminated, siderite-cemented, very fine-grained sandstone	Same as Lithofacies 21 above but with siderite cement, resulting in an orange-grey colour and very well consolidated.		
	23	Argillaceous, very fine- to fine-grained sandstone	Light brown-grey, argillaceous, fine- to very fine-grained sandstone. Grains are sub-angular to sub-rounded and poorly to moderately sorted. Generally well consolidated. Abundant wavy mud laminae.		
	24	Interbedded very fine-grained sandstone and siltstone	Interbedded very fine-grained sandstone (light grey) and siltstone (dark grey). Abundant wavy mud laminae and claystone rip-up clasts.		
	25	Bioturbated siltstone	Dark grey, bioturbated siltstone. Hard, blocky, well consolidated. Common wavy mud laminae. Sometimes very thinly interbedded with mudstone or very fine-grained sandstone. Bioturbation is typically quite intensive, overprinting any primary structure, with horizontal to inclined burrows.		
MUDERONG SHALE / FLAG SANDSTONE	26	Siltstone	Dark grey siltstone. Hard, blocky, well consolidated. Common wavy mud laminae. Sometimes very thinly interbedded with mudstone or very fine-grained sandstone. Rare to common claystone rip-up clasts. Some patches siderite-cemented (orange-grey colour and very well consolidated). Rare siderite or calcareous nodules and floating sand-sized quartz grains.	FACIES ASSOCIATION D	Basin floor fan lobe abandonment or basin floor
	27	Claystone	Dark brown to dark grey claystone. Generally hard, blocky texture, but some fissility. Some patches siderite-cemented (orange-grey colour and very well consolidated). Sometimes very thinly interbedded with siltstone. Rare calcareous nodules and floating sand-sized quartz grains.		

flows and high-density turbidity currents in the proximal to mid fan depositional environment.

6.5.1.3 Facies Association C – Distal Basin Floor Fan or Fan Lobe Waning

Facies Association C comprises lithofacies 19 to 25, and is also representative of the Flag Sandstone. The lithofacies of this association typically overly the coarser-grained sediments of Facies Association B, or are found as independent sequences between the finer-grained sediments of Facies Association D (described below). Fining-upward grading of the sediments is common, indicating decreasing depositional energy. Sedimentary structures include wavy-, parallel- and ripple-lamination, indicating deposition by traction currents. The tops of the beds typically grade into thin siltstone or claystone layers that are formed into flame structures, as a result of sediment loading and dewatering. This association of lithofacies are most likely to have been deposited by low-density turbidity currents. Where they occur in conjunction with the coarser-grained sediments of Facies Association B they are interpreted to represent the waning phase of basin floor fan lobe deposition. Where they occur only in association with the finer-grained sediments of Facies Association D they are more likely to represent distal basin floor fan deposits.

6.5.1.4 Facies Association D – Basin Floor Fan Lobe Abandonment or Basin Floor

Facies Association D comprises lithofacies 26 and 27, and is representative of the lower Muderong Shale and is a minor component within the Flag Sandstone. The siltstones and claystones were deposited by settling out from suspension in a low energy depositional environment. Within the Flag Sandstone, these very fine-grained sediments occur above Facies Association C and are interpreted to be hemipelagic drapes over abandoned basin floor fan lobes. Within the Muderong Shale, the siltstones and claystones do not occur in association with coarser-grained sediments and are therefore interpreted to be basin floor hemipelagic deposits.

6.5.2 Wireline Log Well Correlation

The wells in the Barrow Sub-basin were interpreted in terms of their key stratigraphic surfaces, such as flooding surfaces and sequence boundaries, based on the stacking patterns and wireline log motifs of the gamma ray (GR) and sonic (DT) logs. Key sequence stratigraphic surfaces were interpreted between the *P. iehiense* and *O. operculata* palynological zones of the Early Cretaceous. Figure 6.17 shows an example of the sequence

stratigraphic interpretation of Whitlock-1. The wells were then correlated across the area using a combination of the biozonation information, the interpreted depositional environments, the seismic stratigraphic packages and stratal relationships, and the wireline log motifs and key stratigraphic surfaces. Figure 6.18 to Figure 6.22 give examples of the regional well correlation.

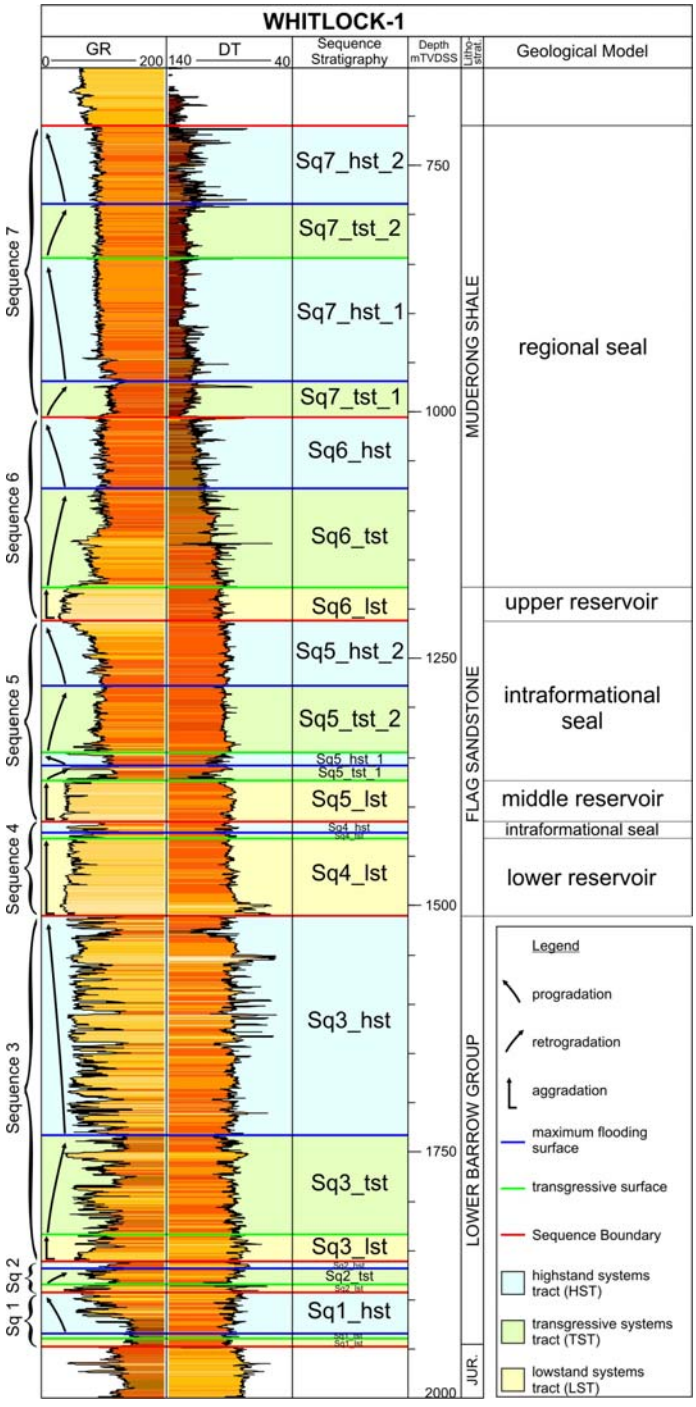

Figure 6.17 Example of the sequence stratigraphic well interpretation of Whitlock-1, highlighting the stacking pattern motifs of the gamma ray (GR) wireline log and the interpreted systems tracts and sequences.

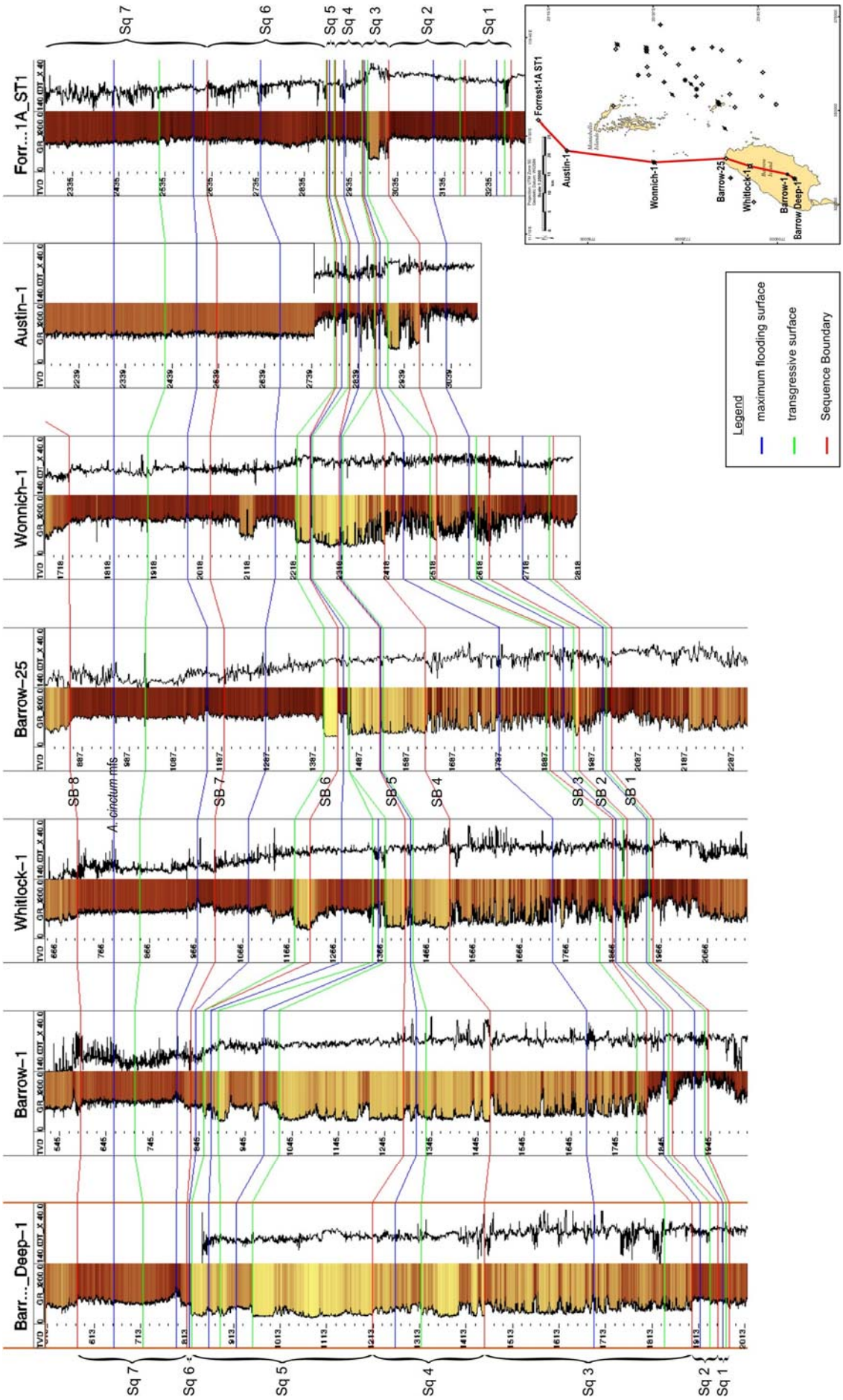

Figure 6.18 Regional well correlation from Barrow Deep-1 to Forrest-1A ST1, depicting the sequence stratigraphic interpretation. The correlation is flattened on the *A. cinctum* maximum flooding surface, near the top of the Muderong Shale regional seal.

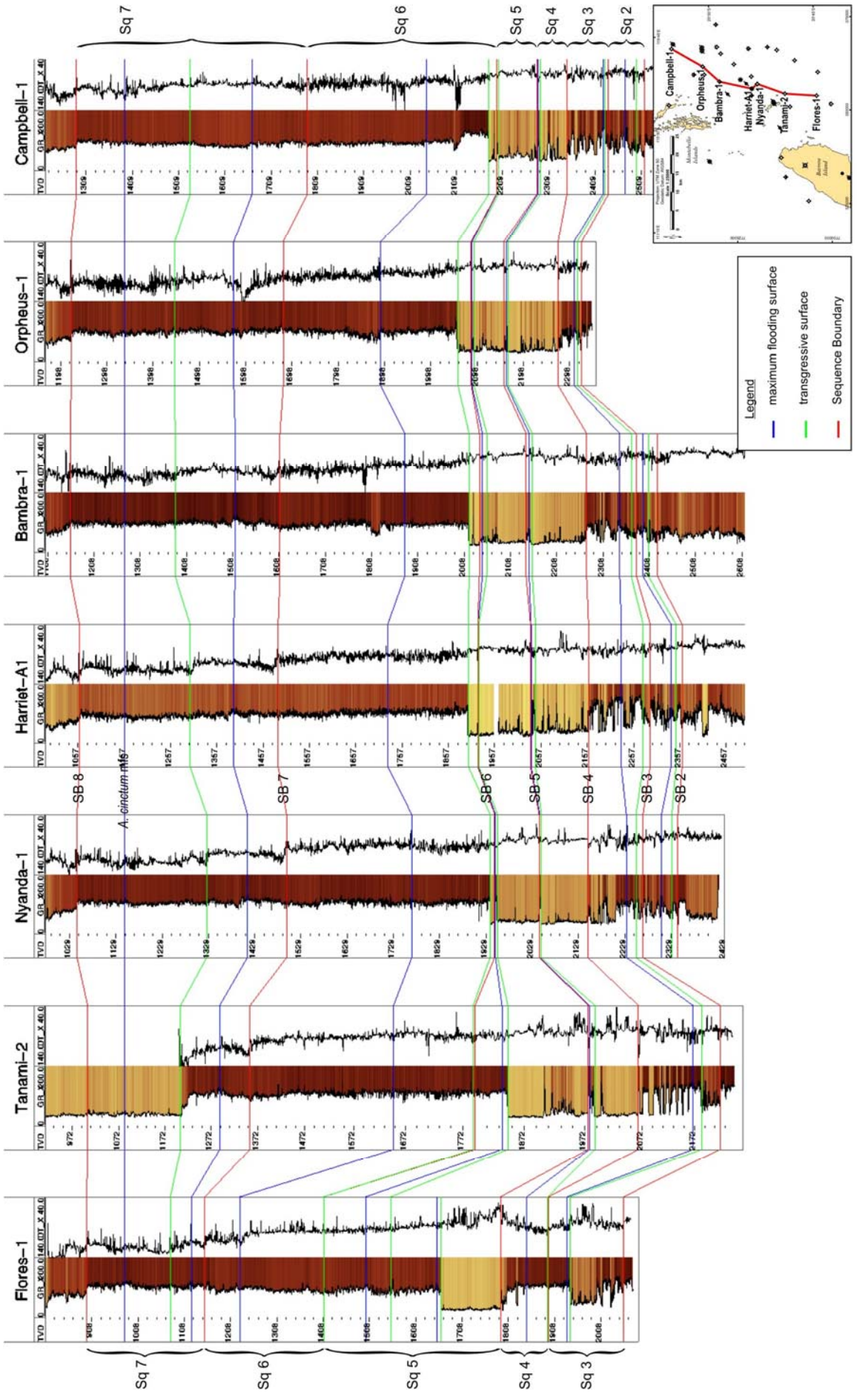

Figure 6.19 Regional well correlation from Flores-1 to Campbell-1, depicting the sequence stratigraphic interpretation. The correlation is flattened on the *A. cinctum* maximum flooding surface, near the top of the Muderong Shale regional seal.

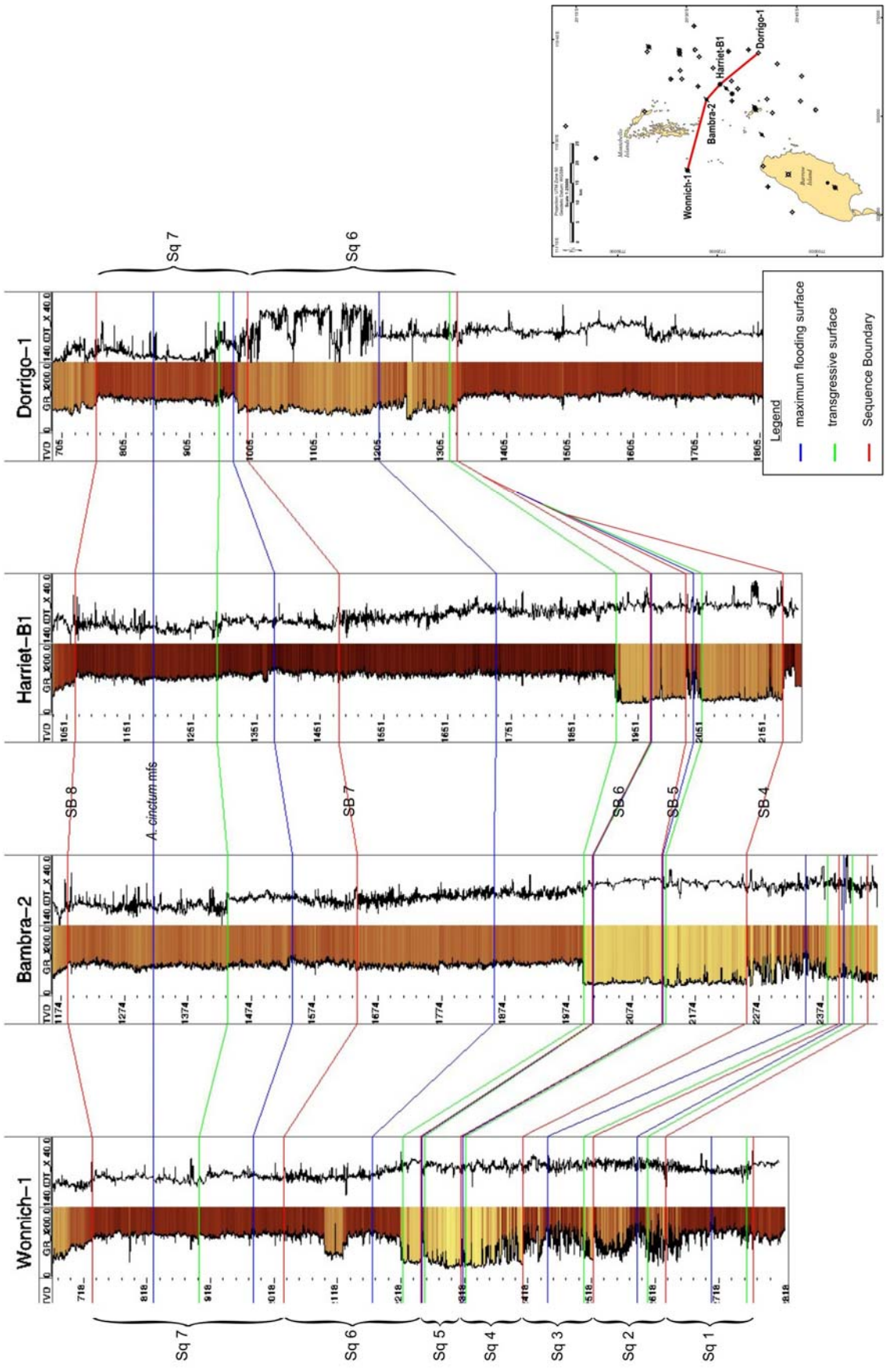

Figure 6.20 Regional well correlation from Wonnich-1 to Dorrigo-1, depicting the sequence stratigraphic interpretation. The correlation is flattened on the *A. cinctum* maximum flooding surface, near the top of the Muderong Shale regional seal.

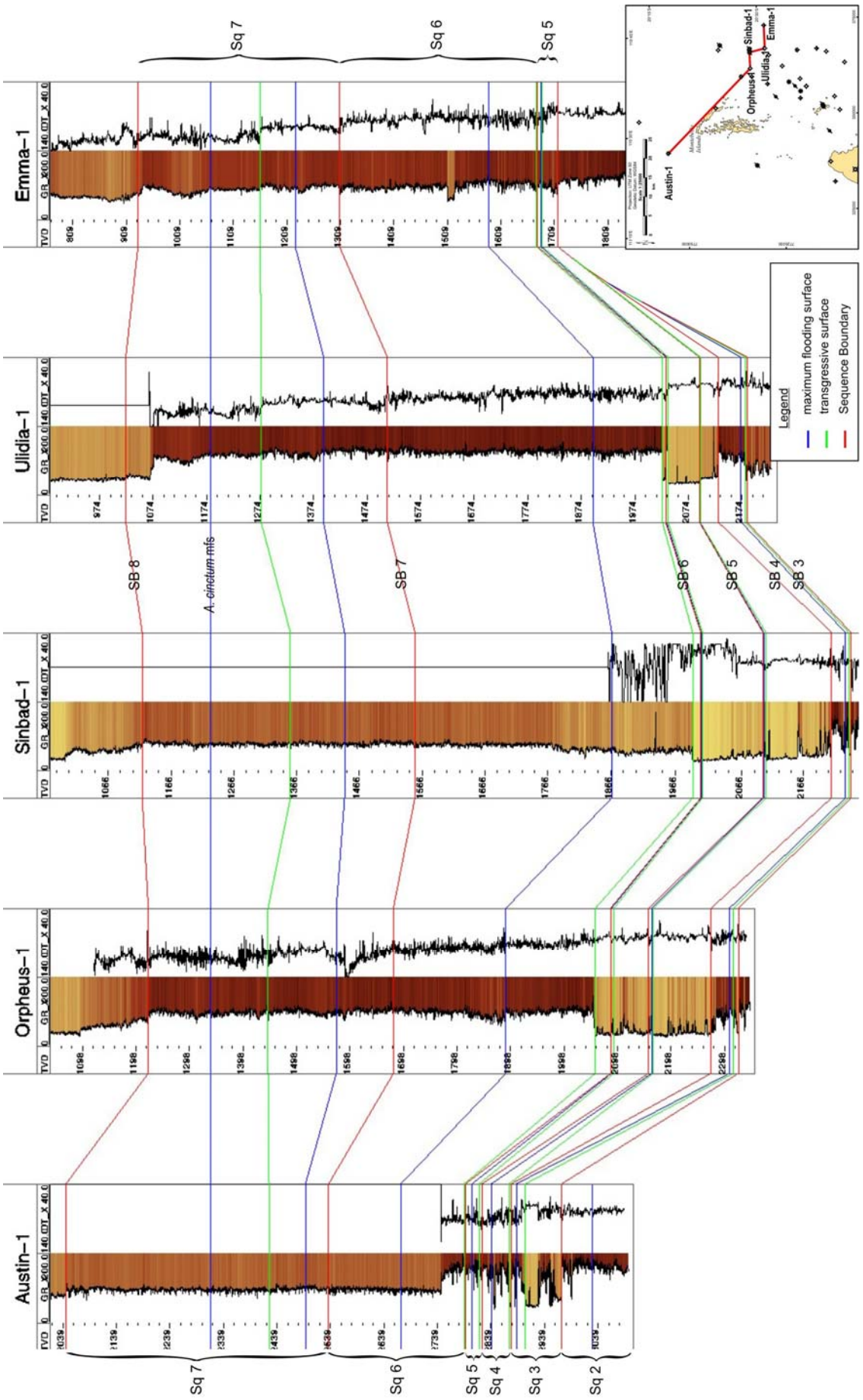

Figure 6.21 Regional well correlation from Austin-1 to Emma-1, depicting the sequence stratigraphic interpretation. The correlation is flattened on the *A. cinctum* maximum flooding surface, near the top of the Muderong Shale regional seal.

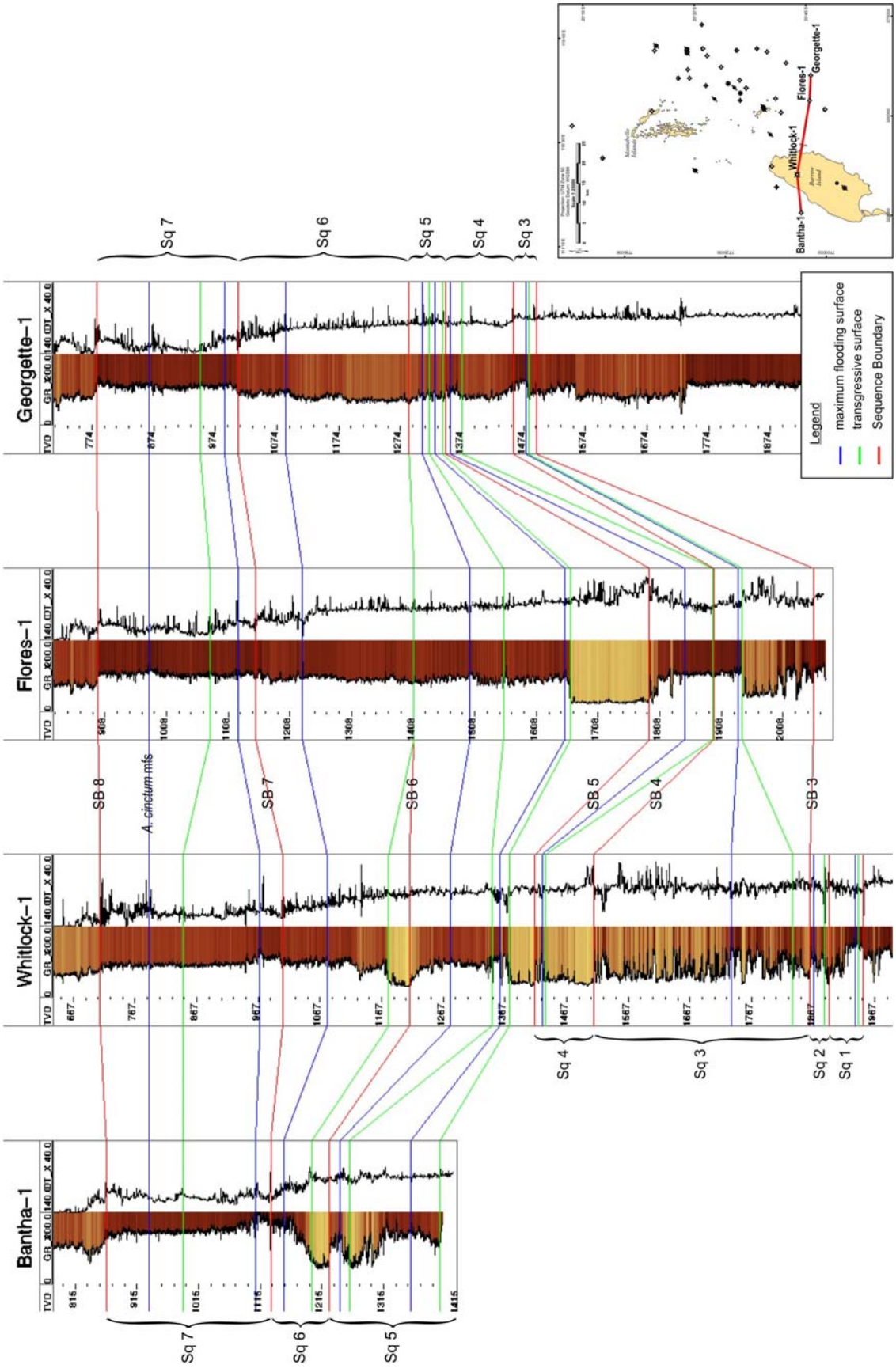

Figure 6.22 Regional well correlation from Bantha-1 to Georgette-1, depicting the sequence stratigraphic interpretation. The correlation is flattened on the *A. cinctum* maximum flooding surface, near the top of the Muderong Shale regional seal.

6.5.3 Sequence Stratigraphy

The integration of seismic structural and stratigraphic interpretations with detailed sedimentological core descriptions, biostratigraphy and wireline log well correlations enabled a sequence stratigraphic framework for the site to be determined. A sequence stratigraphic approach was adopted because it focuses on key surfaces that naturally subdivide the sediment succession into chronostratigraphic units. This is vital to understanding the likely distribution and connectivity of reservoir and seal properties. The approach followed here is that outlined by Posamentier and Allen (1999), where sequences are defined as relatively conformable successions bounded by unconformities or their correlative conformities, and systems tracts are identified by key stratigraphic surfaces and stacking patterns.

Seven unconformity-bound sequences were identified in the Barrow Sub-basin from the base of the Barrow Group to the top Muderong Shale. The sequence stratigraphic interpretation presented here is an updated alternative to that previously proposed by Thompson *et al.* (1990) and (McGilvery, 1996). The sequences and their interpretation are described below.

6.5.3.1 Sequences 1 to 3

Sequence Boundary 1 is the regionally recognised Base Cretaceous Unconformity. Evidence of truncations can be seen on the seismic sections, where the underlying Jurassic strata terminate against the Base Cretaceous Unconformity surface. Sequences 1 to 3 span the *P. iehiense* to *B. reticulatum* palynological zones and are representative of the Malouet Formation (Lower Barrow Group). The Lower Barrow Group sediments are not the focus of this study as they are below the potential injection interval (Flag Sandstone, Upper Barrow Group); however, it was necessary to conduct the interpretation from the base Cretaceous upwards to understand the development of the Barrow Group as a whole.

Sequence 1 is confined to the western part of the study area and each sequence above progressively extends further over to the east, as the Barrow Group successively onlaps onto the Base Cretaceous Unconformity along the eastern and southeastern margins of the Barrow sub-basin (Figure 6.23). The wireline log characteristics through these three sequences depict either high gamma ray (GR), indicating mudstones and shales, or alternating high to low GR signature, suggestive of interbedded sandstones and mudstones. The core descriptions from the well completion reports generally interpret the Malouet Formation to be deepwater marine basinal shales and submarine fan sandstones (Figure 6.24a).

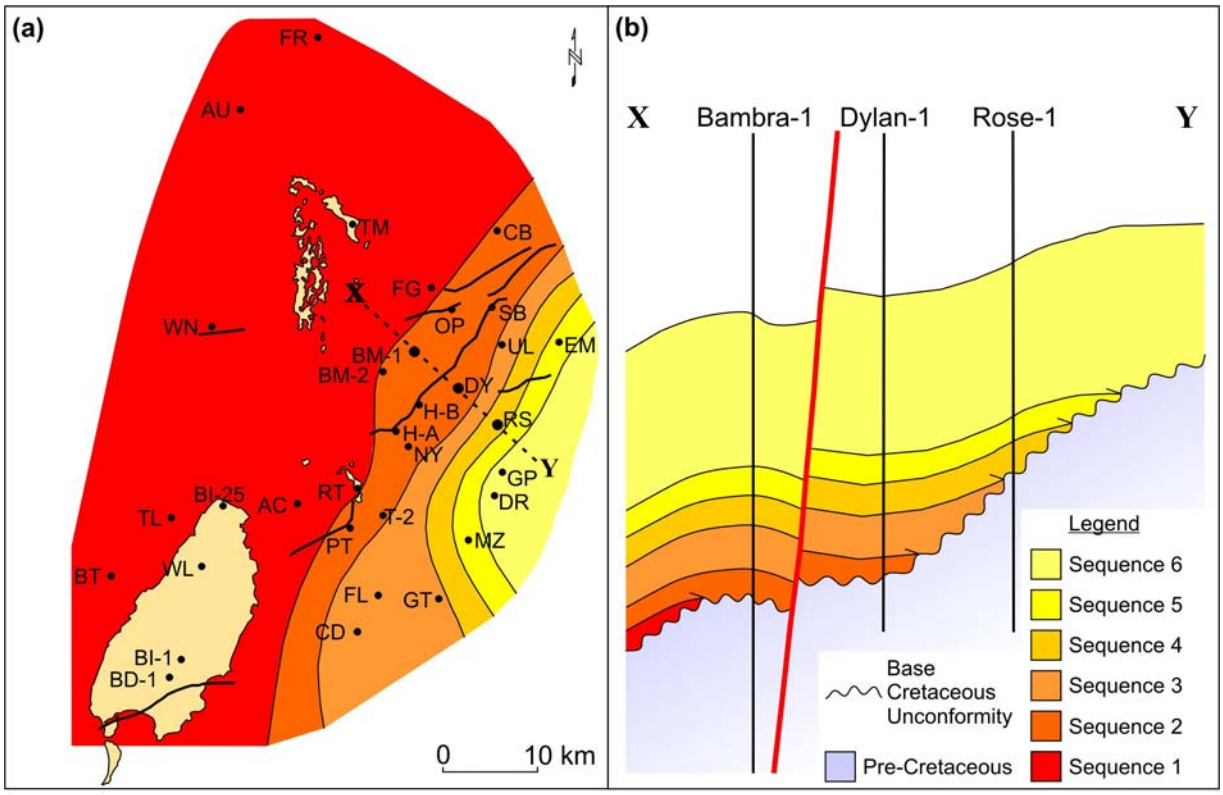

Figure 6.23 Onlap of sequences onto the Base Cretaceous Unconformity (Sequence Boundary 1). (a) Map showing the approximate pinch-out position for each sequence against the Base Cretaceous Unconformity. Each sequence is colour-coded as per the legend shown on part b. (b) Schematic northwest-southeast cross-section (exaggerated vertical scale) highlighting the onlap of the sequences onto the Base Cretaceous Unconformity. The location of the section is shown on part a.

6.5.3.2 Sequence 4

Sequence 4 comprises a thick lowstand systems tract (LST) overlain by a very thin, transgressive systems tract (TST) and highstand systems tract (HST). The sequence spans the *E. torynum* palynological zone and is representative of the lower Flag Sandstone. The base of Sequence 4 is indentified from the well logs by a distinct change in the GR wireline log motif from a high or alternating GR signature to a sharp-based, blocky, low GR signature (Figure 6.17–Figure 6.22). There are no cored intervals through the lower Flag Sandstone, but the cuttings descriptions consist of predominantly medium- to coarse-grained sandstones with minor interbedded siltstones and claystones. The similarities with the overlying upper Flag Sandstone, which is cored, suggest that the sandstones were similarly deposited by sandy debris flows and high-density turbidity currents as a series of stacked, amalgamated basin floor fans. The fans are sourced from the eastern side of Barrow Island and extend out to the north. The distal edges of the fan are seen at Austin-1 and Forrest-1A ST1 (Figure 6.24b and d).

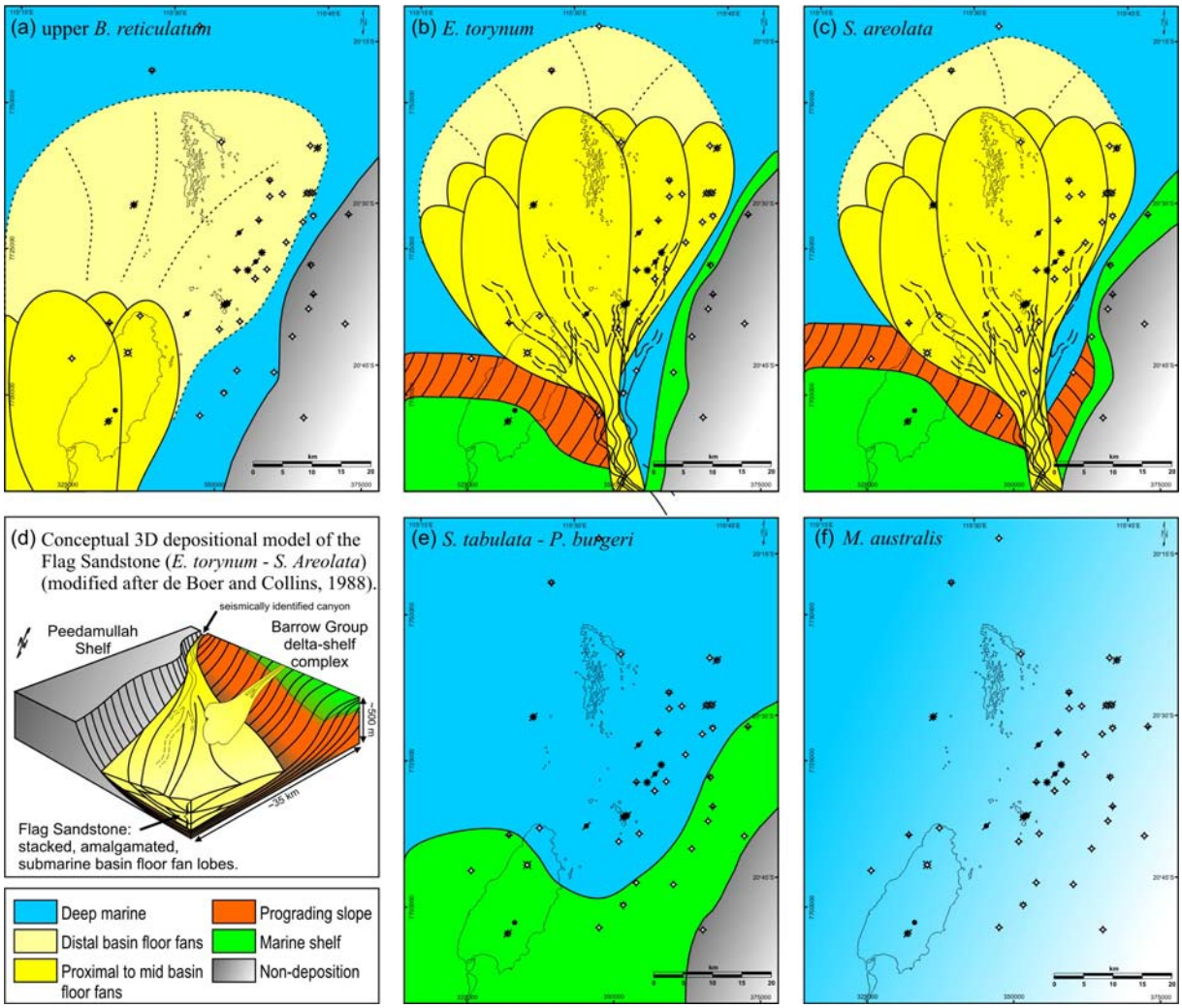

Figure 6.24 Series of regional palaeogeography maps, highlighting the different depositional environments at various points in time through the sequence stratigraphic interpretation.

6.5.3.3 Sequence 5

Sequence 5 comprises a thick LST very similar to that of Sequence 4, and two transgressive-regressive cycles of TST and HST. The sequence spans the *S. areolata* palynological zone and is representative of the upper Flag Sandstone. The LST is present across the majority of the study area and is identified on well logs by a return to a low GR wireline log motif. The numerous sedimentary cores through this LST were interpreted as basin floor fan sandstones, deposited by sandy debris flows and turbidity currents (Figure 6.24c and d). The lower TST-HST cycle of Sequence 5 occurs only in the southern part of the study area, at Barrow Island and along the southeastern sub-basin margin (Figure 6.17–Figure 6.22). A progradational seismic facies is seen on the seismic data between Bantha-1 and Triller-1, and is interpreted as a northward-prograding shelf margin (Figure 6.8). A second

cycle of transgression and regression is recorded over the whole study area, thickest at the northern end of Barrow Island, where it represents continued shelf-scale progradation.

6.5.3.4 Sequence 6

Sequence 6 comprises a thin LST and thick TST and HST. The LST represents the uppermost Flag Sandstone, whilst the TST and HST represent the Mardie Greensand Member and Muderong Shale. The sequence spans the upper *S. areolata* to *M. testudinaria* palynological zones. A down-step in the progradational seismic facies (up-dip of Bantha-1 on the North West Barrow 3D survey, Figure 6.8) is interpreted to be the result of a fall in relative sea level, marked by Sequence Boundary 6 (*S. areolata*, Flag Sandstone). The LST is absent in the southern part of the study area, which is probably the result of sediment bypass and subaerial exposure of the shelf, with deposition occurring as another series of basin floor fan lobes over the rest of the study area. The thick TST and HST of Sequence 6 (*S. tabulata – M. testudinaria*, Muderong Shale) correspond to the onset of widespread transgression and the deposition of shelf sandstones of the Mardie Greensand Member and basinal marine shales of the Muderong Shale (Figure 6.24e).

6.5.3.5 Sequence 7

Sequence Boundary 7 is the regionally recognised intra-Muderong hiatus. The palynology data lack sufficient resolution to indicate a hiatus in deposition; however, the seismic data show evidence of an erosional truncation. Sequence 7 spans the *M. australis* to *O. operculata* palynological zones and is representative of the upper Muderong Shale. Sequence 7 does not contain a LST in the area studied, but instead comprises two transgressive-regressive cycles of TST and HST, corresponding to the continued relative sea level rise and flooding of the previous marine shelf (Figure 6.24f). Sequence Boundary 8 occurs at the top of the Muderong Shale and is representative of the regionally recognised Aptian unconformity.

6.6 INJECTIVITY

Upon injection into a reservoir rock, the flow behaviour and migration of CO_2 will depend primarily on parameters such as the injection rate, viscosity ratio and relative permeability, but is also influenced by the stratigraphic architecture, reservoir heterogeneity and structural configuration of the rocks. Factors affecting injectivity that can be assessed through the

geological characterisation therefore include the reservoir's quality, geometry and connectivity.

6.6.1 Reservoir Quality

6.6.1.1 Porosity and Permeability

Core plug porosity and permeability data are plentiful over the Flag Sandstone and demonstrate a range of reservoir quality (Figure 6.25 and Appendix D). The Flag Sandstone sediments have porosities of 3–29 % and permeabilities of 0.01–7000 mD, with the majority of the data points in the 15–25 % porosity range and 100–5000 mD permeability range, indicating good to excellent reservoir quality. The Flacourt Formation only has a few core data points, but these also exhibit similar high reservoir quality (Figure 6.25). The Mardie Greensand Member, however, shows rather different reservoir quality (Figure 6.25). The porosity similarly ranges up to 30 % but the permeability is only 1 mD or less, indicating that reservoir quality is very poor and that fluid flow through the Mardie Greensand Member will be much more difficult, if at all possible. As the Mardie Greensand Member is not the planned injection formation, this is not too much of a concern. The implication of this poor reservoir quality, however, is that CO_2 migrating up-dip is not likely to enter this formation if other more permeable sediments exist.

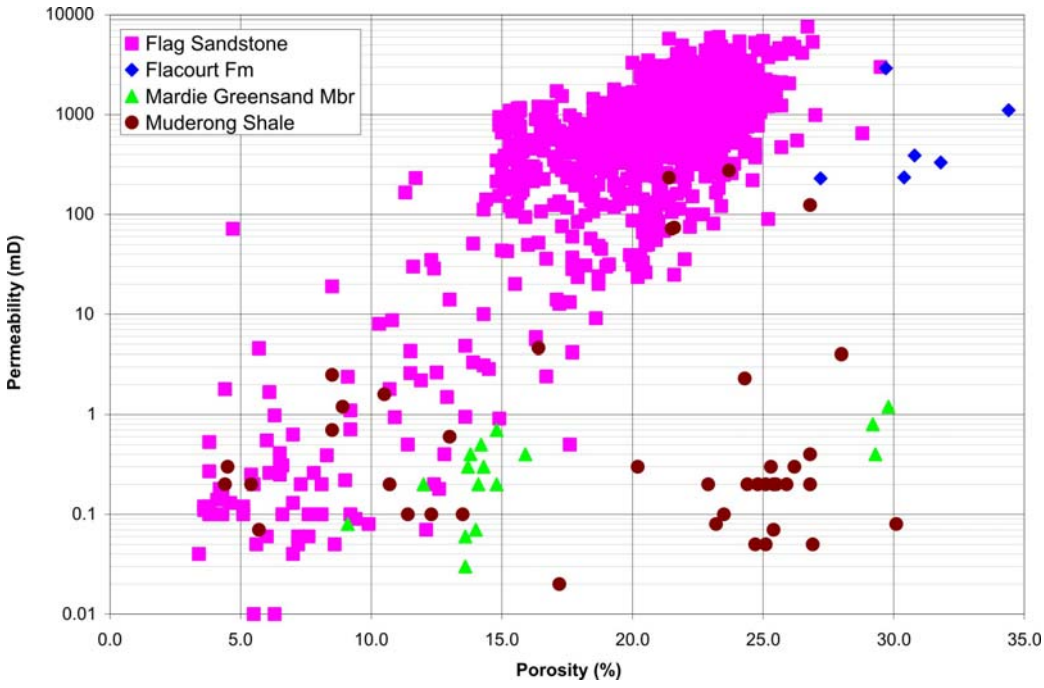

Figure 6.25 Core plug porosity and permeability data from the Barrow Sub-basin, discriminated by formation.

As the Flag Sandstone has such a large core plug dataset, further analysis was undertaken to characterise the porosity and permeability distributions within the reservoir. The detailed sedimentological assessment (discussed earlier in section 6.5.1) resulted in the identification of 27 lithofacies (based on variations in grain size, composition and sedimentary structures), which were then grouped into four facies associations (Figure 6.26). The scatter plot of porosity versus permeability when discriminated by these facies associations indicates groupings of porosity/permeability characteristics. The poorest quality rocks, with typically less than 10 % porosity and less than 10 mD permeability, are the fine-grained basin floor or lobe abandonment sediments. The distal basin floor fan sediments show a wide range in reservoir quality from poor to good. The best reservoir quality sediments, with porosities typically greater than 15 % and permeabilities in the 100s to 1000s mD range, are the proximal to mid basin floor fan sediments. A statistical analysis of the Flag Sandstone core plug samples (Table 6.3) indicates that about three-quarters of the Flag Sandstone consists of Facies Association B(i), the medium- to very coarse-grained, poorly to moderately sorted, massive sandstones. The high abundance of these sediments, with porosities of 15 to 25 % (average 21 %) and permeabilities typically in the mid hundreds to low thousands of mD (average 1343 mD), demonstrate that the Flag Sandstone has exceptionally high reservoir quality, which will be very suitable for CO_2 injection.

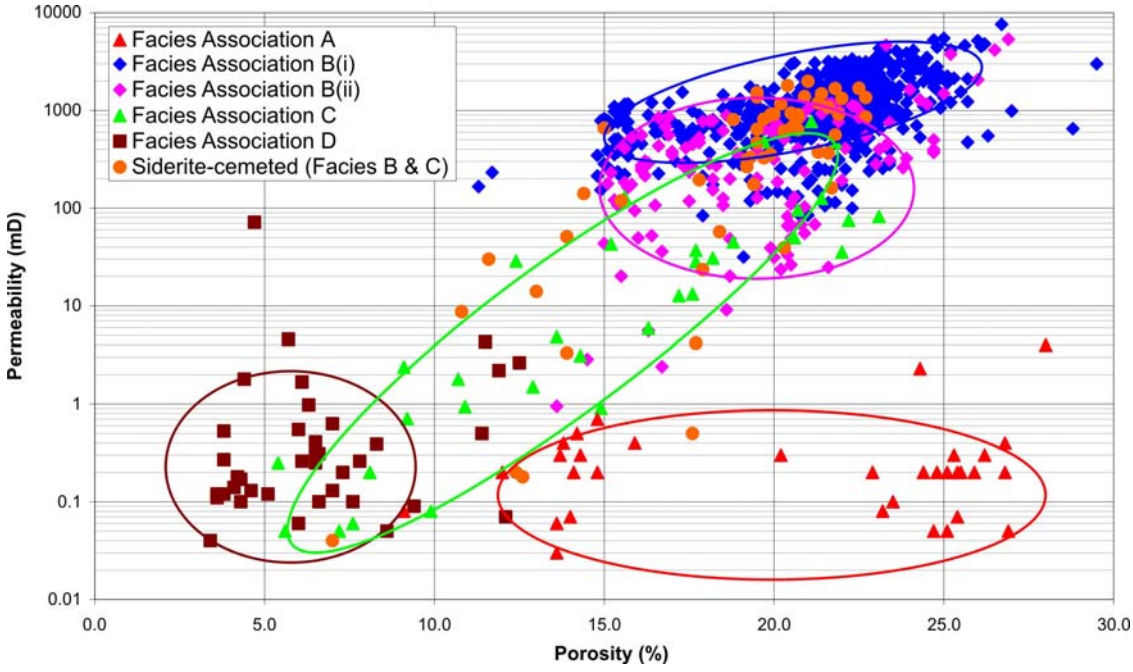

Figure 6.26 Core plug porosity and permeability data from the Barrow Sub-basin, discriminated by facies association (Facies Association B divided into B(i) medium- to very coarse-grained, massive sandstone lithofacies only and B(ii) fine- to medium-grained sandstones with higher mud matrix content, sedimentary structures or dewatering features).

Table 6.3 Abundance, average porosity and permeability for Facies Associations within the Flag Sandstone.

Facies Association	Number of Samples	Abundance (%)	Porosity (%)	Permeability (mD)
A – Mid to Outer Shelf	34	Non-Flag Sandstone		
B (i) † – Proximal to Mid Basin Floor Fan	694	73	21.3	1342.8
B (ii) † – Proximal to Mid Basin Floor Fan	132	14	19.3	541.7
C – Distal Basin Floor Fan or Fan Lobe Waning	33	3	15.1	86.4
D – Basin Floor Fan Lobe Abandonment/Basin Floor	38	4	8.4	6.5
Siderite-Cemented Lithofacies (Facies Ass. B & C)	56	6	18.9	656.2
Total/Average	**987**	**100**	**20.1**	**1095.4**

† B(i) consists of medium- to very coarse-grained, massive sandstone lithofacies only and B(ii) consists of fine- to medium-grained sandstones with higher mud matrix content, sedimentary structures or dewatering features.

6.6.1.2 Petrographic Characterisation

A petrographic assessment, including thin section description, modal composition analysis, X-ray diffraction bulk/clay mineralogy and scanning electron microscopy (SEM), was conducted on core samples from 16 wells within the study area (Kraishan *et al.*, 2003). Of the reservoir sandstones (Flag Sandstone), four distinct lithofacies were sampled. The primary lithofacies was the medium-grained, poorly sorted, massive sandstone. The other lithofacies studied included fine-grained, laminated sandstone, siderite-cemented, medium-grained, poorly sorted, massive sandstone, and fine-grained, argillaceous sandstone.

The pore-scale petrographic characterisation determined that the framework composition of the Flag Sandstone sediments is typically monocrystalline quartz, with minor to moderate amounts of feldspar and trace amounts of rock fragments (mainly chert). The Flag Sandstone is classified as quartzarenite, subarkose, arkose and sublitharenite. The majority of the samples are subarkose and the average framework grain composition is $Q_{85.7}\,F_{12.6}\,R_{1.6}$ (Figure 6.27). Potassium feldspars, such as orthoclase, dominate the feldspar fraction. Other trace to minor components within the samples include micas, glaucony, calcite, dolomite, siderite, pyrite and various clay minerals. Trace amounts of organic matter were also found.

Quartz-overgrowth and siderite are the two main types of authigenic cements within the samples. The siderite cement is the earlier in the diagenetic history, and occurs as a fine, grain-coating cement (Figure 6.28). The later quartz overgrowth cement occurs as thin to occasionally thick, euhedral overgrowths (Figure 6.28). Kaolinite cement is also present in many of the samples and occurs as pseudo hexagonal book-like crystals, filling some of the pore spaces and locally restricting the reservoir quality (Figure 6.28). Other minor authigenic

Figure 6.27 QRF ternary diagram showing framework grain composition of the Flag Sandstone. The axes of the diagram are: quartz (Q) = 100%, feldspars (F) = 50 % and rock fragments (R) = 50 % (modified after Kraishan *et al.*, 2003).

minerals include illite, illite-smectite, smectite and dolomite. Alteration of the feldspars into clay minerals, predominantly kaolin and occasionally illite, can also be seen.

The visual porosity of the studied samples is dominantly primary intergranular porosity. Secondary porosity has mostly resulted from partial to complete dissolution of potassium feldspar (Figure 6.28). Both compaction and cementation processes have played roles in reducing the original intergranular porosity. In particular, primary intergranular porosity within the reservoir is locally restricted by the presence of authigenic minerals, including quartz overgrowth and siderite cements and pore-filling kaolin clay minerals (Figure 6.28). However, the point count estimates of visual porosity still indicate that moderate to excellent porosity is generally preserved (with the exception of the argillaceous sandstones).

6.6.1.3 Potential Impact of CO_2-Water-Rock Interactions on Reservoir Quality

CO_2 dissolution into the formation water allows CO_2-water-rock interactions, which will alter the mineralogy and potentially alter the physical aspects of the rock. This can have important implications for injectivity, as mineral dissolution may lead to migration of fine clay minerals and sand grains, or precipitation of new minerals, either of which can block or occlude the porosity and permeability of the reservoir rock.

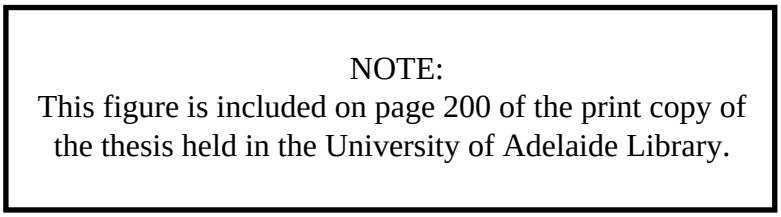

Figure 6.28 Selection of thin section and scanning electron microscope photomicrographs, highlighting reservoir quality of the Flag Sandstone (modified after Kraishan *et al.*, 2003).

The petrographic study indicated that the reservoir units of the Flag Sandstone lack minerals that are reactive to CO_2. Whilst feldspars do make up a minor to moderate component of the formation mineralogy, the chemical composition of the feldspars is not optimal for CO_2-water-rock interactions that will precipitate carbonate minerals. The potential mineral reaction that could occur following the injection of CO_2 is the alteration of potassium feldspar to kaolin and quartz, as shown below (Eq. 11) (Watson & Tingate, 2003):

$$2KAlSi_3O_8 + 3H_2O + 2CO_2 = Al_2Si_2O_5(OH)_4 + 4SiO_2 + 2KHCO_{3\,(aq)} \quad [11]$$

(Potassium feldspar + water + carbon dioxide = kaolin + quartz + potassium bicarbonate in solution)

However, because the feldspars are dominantly alkali, which have a very slow reaction rate, any mineral reactions that do occur are unlikely to be at a rate sufficient to affect injectivity (M. Watson, ASP, pers. comm.). In addition, the authigenic cement is predominantly quartz and dissolution of this cement by injected CO_2 is unlikely. The minor amounts of siderite cement are also likely to be fairly stable in the presence of injected CO_2; however, this is dependent on the formation water chemistry (M. Watson, ASP, pers. comm.).

6.6.2 Reservoir Geometry and Connectivity

The Flag Sandstone and its lateral equivalents (Sequence 4 to Sequence 6 LST) extend across the whole study area (Barrow Island trend and Harriet-Campbell area). The reservoir is thickest in the southern area over Barrow Island, reaching a maximum thickness of 630 m at Barrow Deep-1 (Figure 6.29). It thins towards the eastern sub-basin margin as it successively onlaps the base Cretaceous unconformity, and thins to the north to approximately 80 m at Forrest-1A ST1. The unit is dominantly a medium- to coarse-grained, massive sandstone, with minor interbedded siltstone and claystone. Northwards of the Wonnich field, a lateral facies change takes place over 25–30 km into siltstone and claystone with thin interbeds of medium-grained sandstone (e.g. Austin-1 and Forrest-1A ST1), representing the distal edge of the basin floor fans. Towards the southeastern and eastern sub-basin margins the reservoir becomes finer grained and more glauconitic and argillaceous.

The sand-rich nature of the stacked and amalgamated basin floor fan lobe sediments suggests that connectivity is likely to be excellent. At the field scale, however, there is some evidence to suggest that the regionally extensive tabular sand body of the Flag Sandstone maybe slightly more compartmentalised. For example, the Harriet Field comprises three discrete hydrocarbon accumulations, with slightly different water-hydrocarbon contacts in

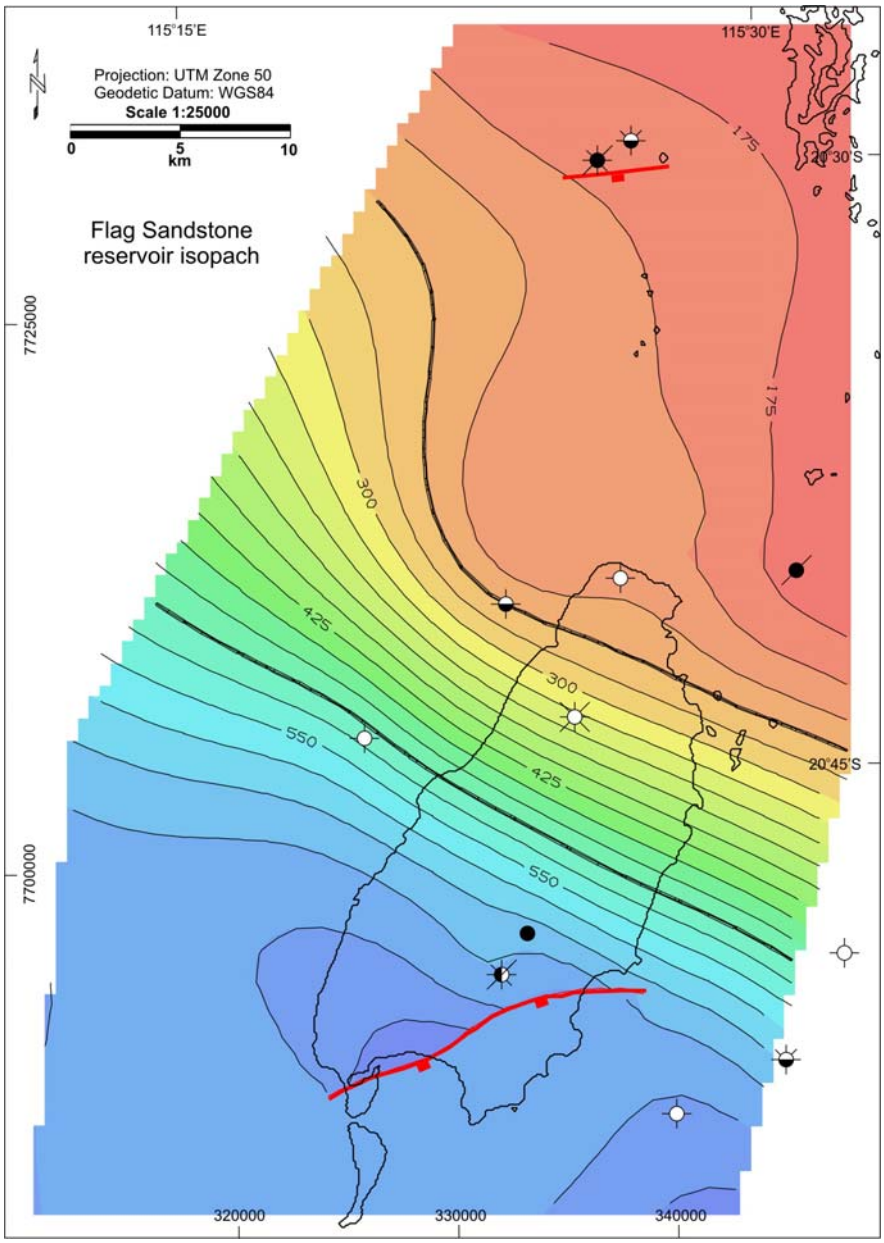

Figure 6.29 Isopach map of the Flag Sandstone reservoir, showing increasing thickness to the southwest.

each. This disconnection is attributed to the likely presence of shale beds preserved on the flanks of the abandoned lobe surfaces (Osborne & Howell, 1987; Howell, 1988; Scott *et al.*, 1992). In addition, the absence of significant water coning during production is attributed to reservoir-scale impediments to otherwise relatively high vertical permeabilities, such as claystone layers between individual fan lobes and siderite-cemented layers (Osborne & Howell, 1987; de Boer & Collins, 1988; Howell, 1988). Thus, the apparent homogeneous nature of the Flag Sandstone on a regional scale can be misleading, as the evidence suggests the formation is considerably more heterogeneous. Connectivity is still likely to be excellent on a regional or long-term time scale, but on a local or injection time scale hemipelagic shale

drapes may restrict the vertical connectivity.

6.7 CONTAINMENT

Supercritical CO_2 is less dense than water (before dissolution); therefore, it will rise buoyantly through the water column. Consequently, containment could be breached by unwanted vertical fluid migration through the top seal, faults/fractures and existing well penetrations. Containment issues that can be assessed through the geological characterisation therefore include the extent, continuity and capacity of the seal, the likely migration pathways and trapping mechanisms, and the geomechanical integrity of the reservoir and seal.

6.7.1 Seal Distribution and Continuity

The Muderong Shale regional seal (Sequence 6 TST to Sequence 7) extends across the whole study area (Barrow Island trend and Harriet-Campbell area). The seal is thickest in the central eastern area, reaching a maximum of just over 1000 m at Dylan-1. It thins towards the southeast and south, to about 500 m at Georgette-1 and Menzies-1 in the southeast, and to about 150 m at its thinnest point on the western side of the Barrow Island to the south. Figure 6.30 displays the Muderong Shale isopach in the Barrow Island trend area, which clearly shows the thick part of the seal immediately to the south of the Wonnich field (~800 m) and the southwards thinning towards Barrow Island (~250 m at Barrow Deep-1). The unit is described on the basis of core and cuttings as a dominantly dark grey claystone and siltstone, with minor interbedded argillaceous sandstone, limestone and dolomite. Towards the eastern and southeastern sub-basin margins it becomes more glauconitic. Despite the variation in thickness, the Muderong Shale is laterally continuous as it extends well beyond the boundaries of the study area. Therefore, on the basis of its distribution and continuity, the Muderong Shale is likely to be a suitable seal for containment of CO_2.

6.7.2 Seal Capacity

The maximum CO_2 column height that a seal is capable of retaining is an important aspect for assessing the quality of the seal. The potential seal capacity of the Muderong Shale regional seal and intraformational seals within the Flag Sandstone were calculated using mercury injection capillary pressure (MICP) analysis. MICP tests are a measurement of the pressures required to move mercury through the pore network system of a core sample. Using the techniques described earlier in Chapter 3, the mercury/air capillary pressure data were

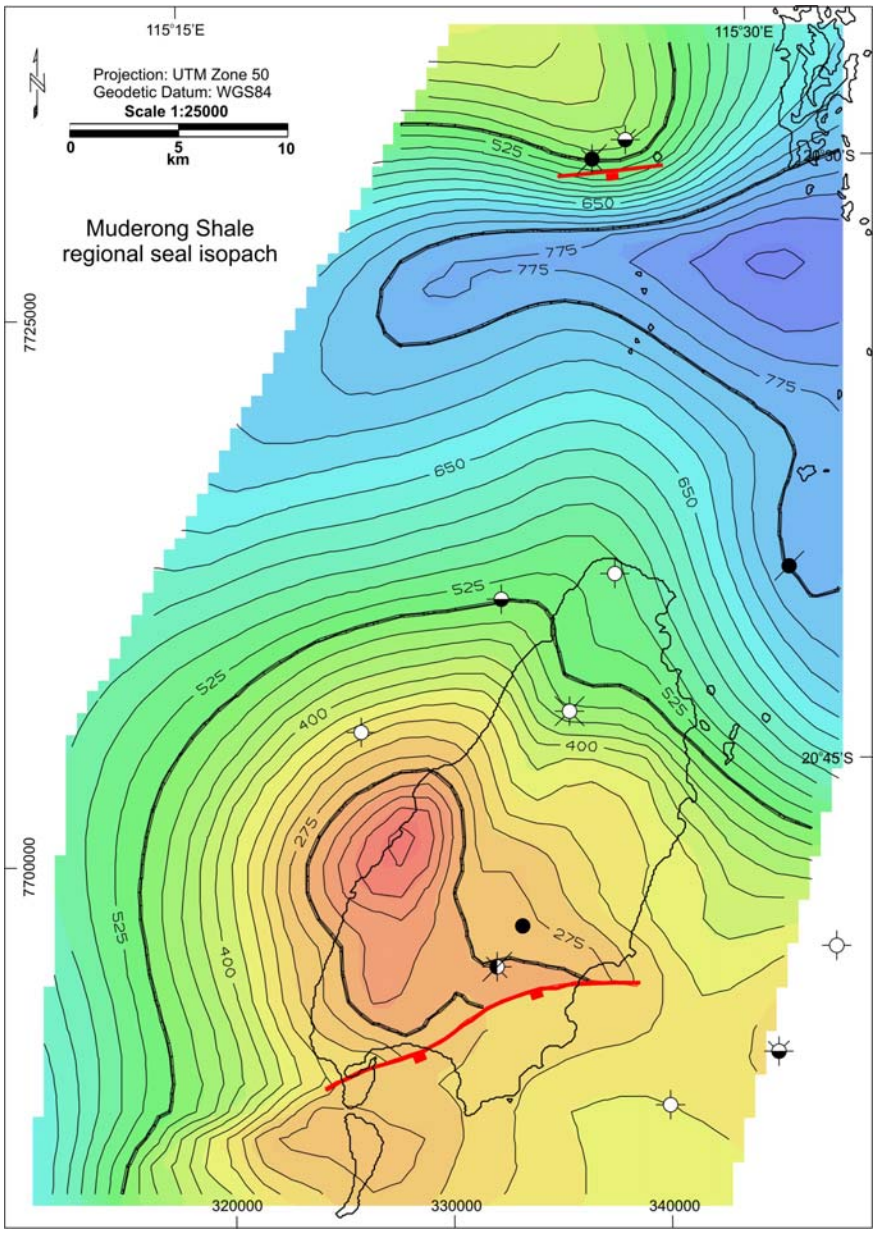

Figure 6.30 Isopach map of the Muderong Shale regional seal, which is thickest near the Montebello Islands and thins to the south over Barrow Island.

translated to equivalent CO_2/water data at reservoir conditions and then converted into seal capacity for CO_2, expressed as the column height that the rock would be capable of holding (sealing). Figure 6.31 shows examples of the mercury intrusion graphs for three of the seal samples, indicating the interpreted threshold pressure points (the mercury intrusion graphs for all samples are shown in Appendix E). The calculated column heights for each of the samples tested are listed in Table 6.4.

The results of the MICP analyses indicate that the basal Muderong Shale (samples from Nyanda-1 and Trimouille-1) has excellent seal capacity, with the potential to hold back CO_2

Table 6.4 CO_2 column heights calculated from MICP analysis.

Well Name	Depth TVDSS (m)	Press. (MPa)	Temp (°C)	CO_2 Density (g/cm^3)	Brine Density (g/cm^3)	Interfac. Tension (mN/m)	Seal P_{th} Hg-air (psia)	Seal P_{th} CO_2-H_2O (psia)	Column Height (m)
Alkimos-1	1889.08	18.5	98.1	0.4483	0.9895	27.71	9971.72	751.47	977
Austin-1	2848.92	27.9	115.0	0.5732	0.9816	24.39	4988.07	330.86	570
Campbe.-2	2176.27	21.3	91.1	0.5589	0.9954	26.67	4982.37	361.38	582
Dorrigo-1	946.89	9.3	49.7	0.3134	1.0140	30.02	340.80	27.82	27
Dorrigo-1	957.41	9.4	50.1	0.3189	1.0138	29.87	238.88	19.41	19
Dorrigo-1	959.46	9.4	50.1	0.3189	1.0138	29.87	4.19	0.34	0
Flag-1	1271.59	12.5	63.6	0.4296	1.0082	28.22	39.92	3.06	3
Flag-1	1273.60	12.5	63.6	0.4296	1.0082	28.22	290.81	22.32	27
Flag-1	2194.58	21.5	95.2	0.5416	0.9928	26.61	6974.80	504.76	787
Harriet-A5	1826.18	17.9	82.6	0.5183	0.9994	27.36	6970.70	518.68	758
Harriet-B1	1915.94	18.8	83.8	0.5377	0.9990	27.14	5004.81	369.41	563
Marra-1	1968.55	19.3	87.5	0.5290	0.9969	27.11	4999.08	368.58	554
Nyanda-1	1922.98	18.8	85.4	0.5276	0.9980	27.20	6965.11	515.23	770
Nyanda-1	1924.27	18.9	85.5	0.5299	0.9980	27.17	6978.83	515.68	775
Nyanda-1	1925.24	18.9	85.5	0.5299	0.9980	27.17	5997.04	443.13	666
Nyanda-1	1925.87	18.9	85.5	0.5299	0.9980	27.17	5991.00	442.69	665
Orpheus-1	2064.39	20.2	87.4	0.5534	0.9973	26.88	5997.33	438.42	694
Sinbad-2	2019.12	19.8	91.7	0.5183	0.9944	27.05	6966.00	512.46	757
Trimoui.-1	2424.22	23.8	103.1	0.5520	0.9884	25.91	4985.15	351.28	566
Trimoui.-1	2425.85	23.8	103.1	0.5520	0.9884	25.91	6966.95	490.93	791
Ulidia-1	2032.92	19.9	84.5	0.5632	0.9990	26.90	6979.89	510.63	824
Wonnich-1	2248.68	22.0	99.4	0.5319	0.9901	26.43	4306.67	309.56	475

Note: P_{th} = threshold pressure; Salinity = 32189 ppm; contact angle = 0°; reservoir P_{th} Hg-air system = 6.85 psia.

column heights ranging from 565 m to 790 m. The average CO_2 column height retention is 705 m. The maximum height of the structural closure of the fault-bounded Barrow Island anticline is about 180–250 m (180 m = maximum reservoir offset across Barrow Island Fault; 250 m = maximum closing contour against Barrow Island Fault); therefore, the seal capacity of the Muderong Shale is more than sufficient to successfully retain CO_2 beneath it if the structural trap was filled to the maximum spill point. By comparison, the samples from Flag-1 are from a sandstone unit within the top Muderong Shale and the samples from Dorrigo-1 are from the more glauconitic Muderong Shale on the eastern margin. These show that the sandier or more glauconitic Muderong Shale is a poor seal, with a maximum CO_2 column height of 27 m. The sandier interbeds within the Muderong Shale are unlikely to be a

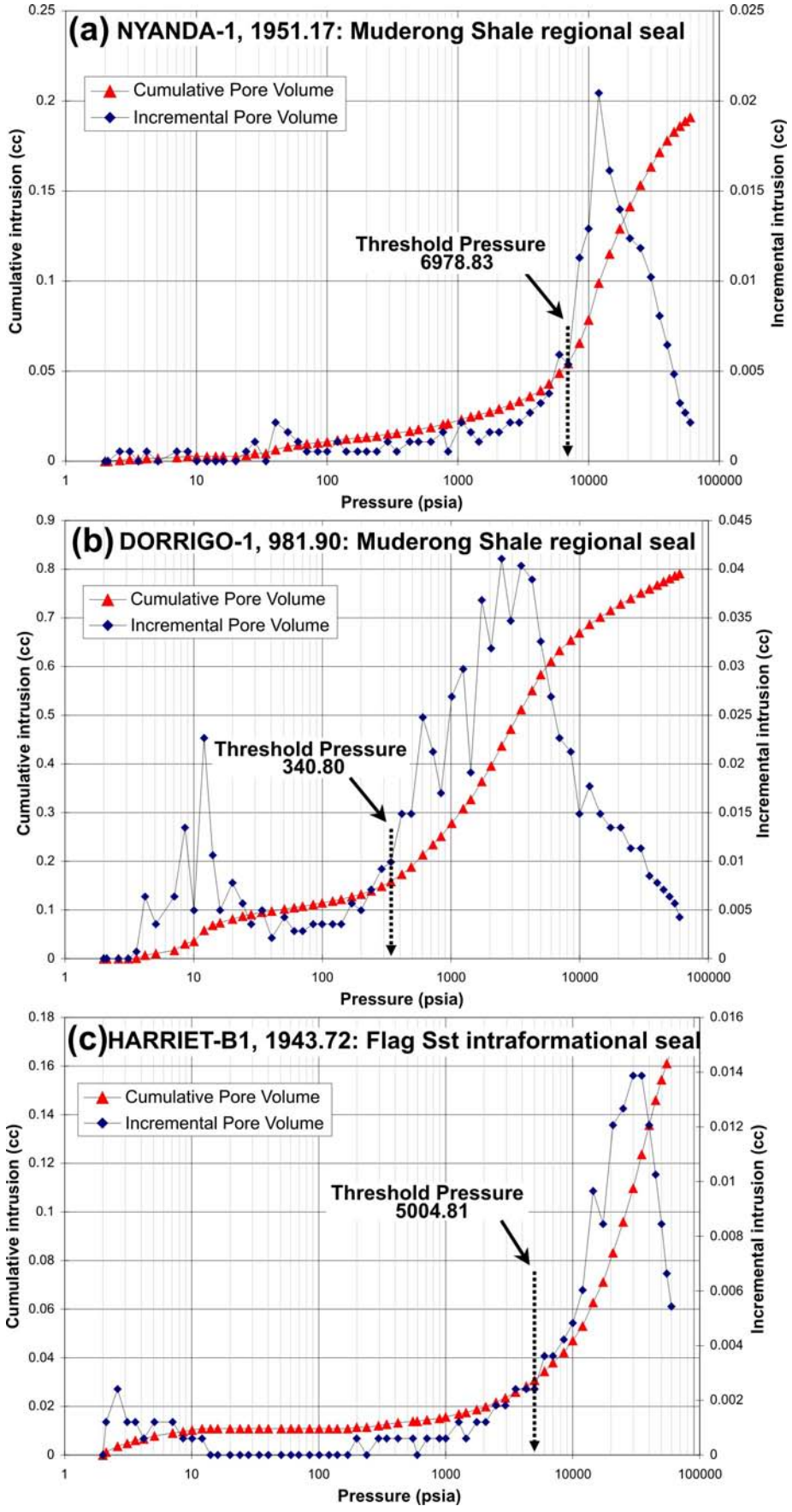

Figure 6.31 Example mercury injection capillary pressure curves highlighting threshold pressure for: (a) & (b) Muderong Shale regional seal (central and eastern, respectively); and (c) intraformational seal.

risk to containment because of the greater coverage of claystones and siltstones, particularly at the base of the Muderong Shale where the containment potential is most critical. However, the lateral change to a more glauconitic facies on the eastern and southeastern sub-basin margins may be a potential risk to containment, but as this is outside the potential CO_2 containment area (the Barrow Island anticline) the risk is considered minimal.

The remaining samples are representative of intraformational seals from within the Flag Sandstone. These are thought to be hemipelagic drapes (up to 2 m thick in the cores viewed), which, although thin, are likely to be laterally extensive (100s m to 1000s m). These have column heights ranging from 475 m to 975 m, with an average CO_2 column height retention of 685 m, and thus have the potential to form significant baffles and barriers to flow, which will hinder or slow the vertical migration of CO_2. The intraformational seals may be beneficial in encouraging the CO_2 to migrate laterally within the reservoir and could thus provide additional containment security by creating small localised traps throughout the succession and by increasing the length of the CO_2 migration pathway (which will result in greater dissolution and residual trapping).

6.7.3 Migration Pathways and Trapping Mechanisms

After injection ceases, the buoyancy of the free-phase (immiscible) CO_2 due to its density will result in it migrating to the highest point in the reservoir. Stratigraphic heterogeneities, such as intraformational siltstones and shales, have the potential to reduce the effective vertical permeability and create a more tortuous migration pathway for injected CO_2. Once CO_2 plume has reached the top of the reservoir, the structural dip and geometry at the base of the overlying seal will have a strong influence on the subsequent migration direction.

The structural geometry of the reservoirs and seals of the Barrow Sub-basin were evaluated earlier in section 6.4.1. The general structural trend of the strata is a northward-plunging fault-bound anticline (Figure 6.12). Flow vectors plotted on the base Muderong Shale regional seal depth surface indicate the up-dip migration directions based on the structural geometry and show how CO_2 will generally migrate southward towards the structural crest of the Barrow Island anticline (Figure 6.32).

The suggested injection location is immediately up-dip (south) of the Wonnich Field. CO_2 is expected to migrate southwards towards Barrow Island, up and along the axial trend of the Barrow Island anticline (Figure 6.32). At Wonnich-1, the Flag Sandstone comprises three sandstone packages (Sequence 4, 5 and 6 LSTs), each separated by a thin shale package

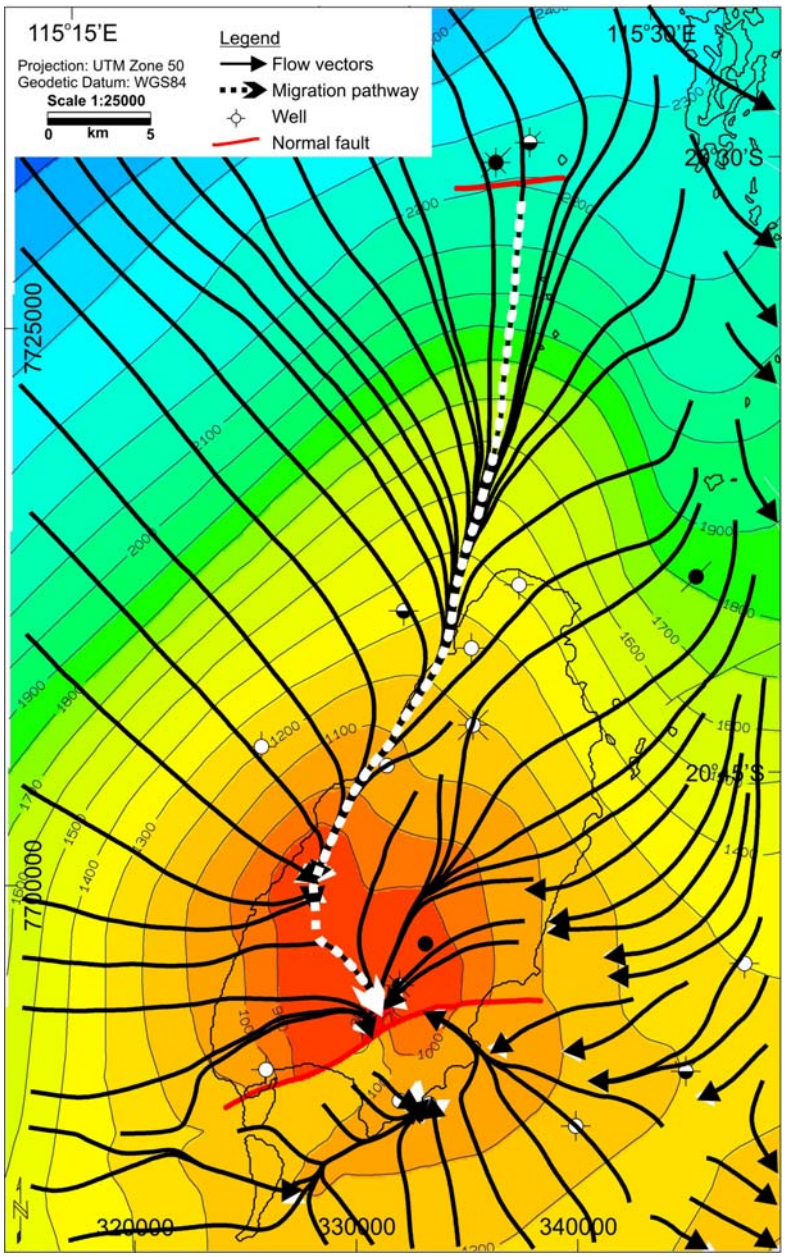

Figure 6.32 Potential CO_2 migration pathways based on the structural geometry of the Base Muderong Shale (base regional seal) depth structure surface. CO_2 migration is expected to occur along the axis of the Barrow Island anticline towards the south if an injection site was located at the nose of the anticline just south of the Wonnich fault. The actual migration pathway is dependent on the exact location of a potential injection site.

(Sequence 4 and 5 TSTs/HSTs) (Figure 6.33). As noted in the MICP analysis, these intraformational seals, although thin, may be very effective barriers to CO_2 migration. The lower shale break (Sequence 4 TST/HST) thickens slightly and the upper shale break (Sequence 5 TSTs/HSTs) thickens significantly towards Barrow Island (Figure 6.33). These intraformational seals also exhibit a lateral facies change towards the south, becoming siltier and sandier. Thus, at the southern end of Barrow Island (e.g. Barrow-1 and Barrow Deep-1)

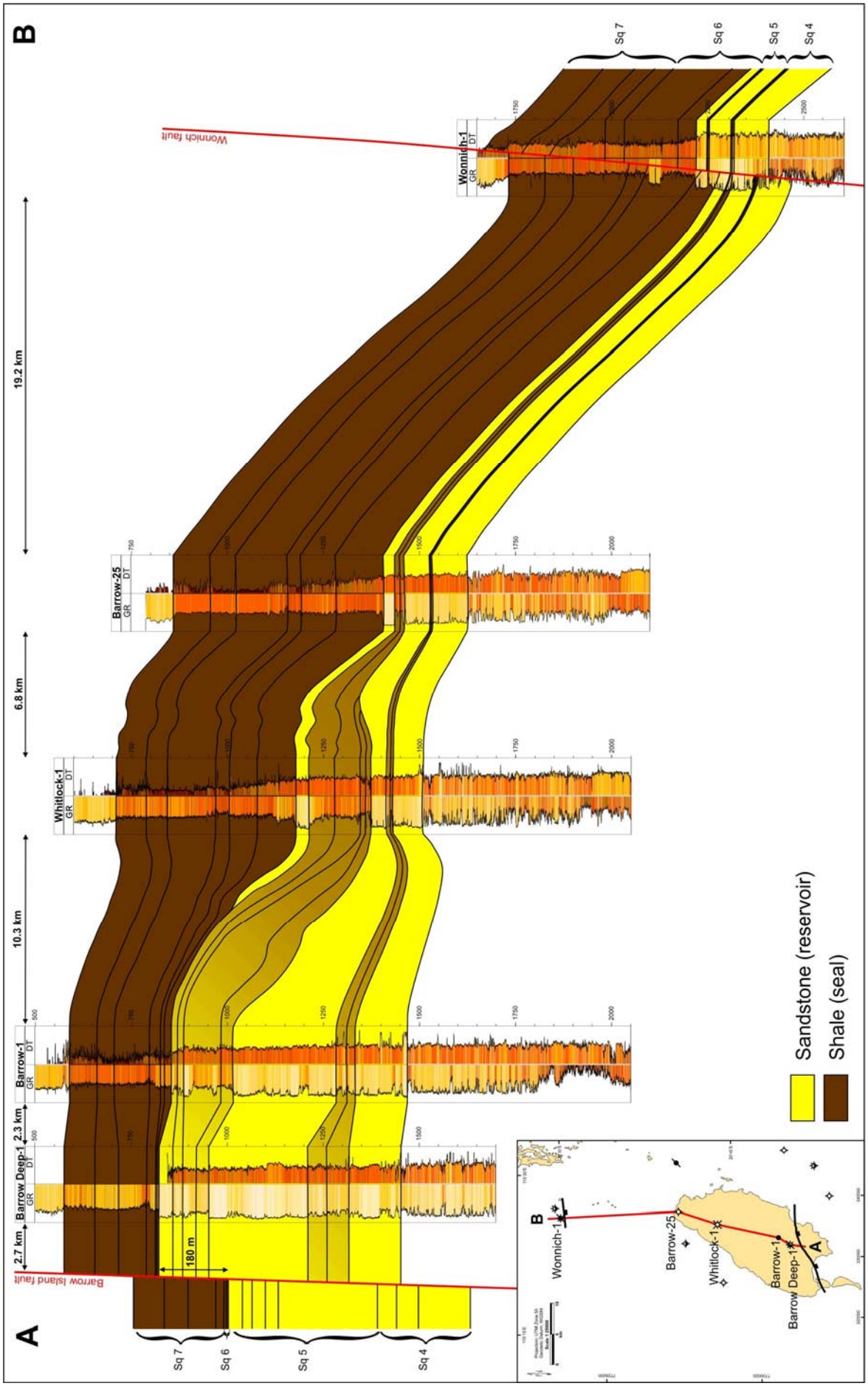

Figure 6.33 Schematic cross-sectional representation of reservoir and seal distribution along the axis of the Barrow Island anticline based on the sequence stratigraphy.

they may no longer act as intraformational seals (Figure 6.33).

Injected CO_2 migrating within the lower and middle Flag Sandstone reservoir units (Sequence 4 and 5 LSTs) is likely to proceed southwards beneath the intraformational seals, until it can diffuse through those seals, and migrate vertically through the reservoir to the base of the Muderong Shale regional seal (Sequence 6 and 7 TSTs/HSTs). The uppermost Flag Sandstone reservoir unit (Sequence 6 LST) pinches out somewhere between Whitlock-1 and Barrow Deep-1 (Figure 6.33). Depending on the sandiness of the underlying intraformational seals at this point (Sequence 5 TSTs/HSTs), CO_2 migrating within the upper Flag Sandstone (Sequence 6 LST) may either become stratigraphically trapped, or may continue to migrate within the unit now underlying the Muderong Shale regional seal (Sequence 5 HST 2). If the CO_2 continues to migrate southwards beneath the Muderong Shale it will ultimately become structurally trapped in the fault-bound anticlinal structure of Barrow Island (Figure 6.33). The trapping mechanisms are therefore likely to be a combination of residual and solubility trapping along the migration pathway, small stratigraphic traps created by the interfingering of basin floor fan sandstones with up-dip continental slope shales, and structural trapping within the fault-bound anticlinal closure of Barrow Island. The distance that a CO_2 plume will migrate southwards from an injection point near Wonnich will depend on the injection rates and volumes, the relative permeability and the tortuosity of the pathway created by the reservoir heterogeneity.

6.7.3.1 Potential for Mineral Trapping of CO_2

CO_2 introduced into the reservoir system will generate long-term CO_2-water-rock interactions. Detailed petrology can provide information on the potential mineral reactions of the CO_2 with the host rock, including dissolution, alteration and precipitation. In certain cases, mineral precipitation can lead to mineral trapping of CO_2 and increased containment security.

The petrographic characterisation by Kraishan *et al.* (2003) determined the mineralogy of the Flag Sandstone reservoir. As discussed above in section 6.6.1.3, the mineralogy of the reservoir units of the Flag Sandstone offers little reactive potential with CO_2. There was some potential for mineral reaction with potassium feldspar (Eq. 11); however, this reaction would precipitate only kaolin and quartz and leave potassium bicarbonate in solution. Contributions of iron or calcium from the formation water and/or other minerals may result in the precipitation of siderite and calcite, dependent on the acidity of the formation water (M.

Watson, ASP, pers. comm.). The Flag Sandstone mineralogy is beneficial in terms of not inhibiting injectivity, but conversely it means that there is limited potential for mineralogical trapping of the CO_2 through precipitation of carbonate minerals.

6.7.4 Geomechanical Assessment of Fault Stability

CO_2 injection into the geological subsurface increases the formation pressure, which can potentially reactivate pre-existing faults or generate new fractures, leading to a possible loss of containment. Geomechanical modelling was undertaken by Streit (2003) to assess the stability of known faults in the Barrow Sub-basin and to estimate maximum sustainable pore fluid pressures for CO_2 injection that will not induce fault reactivation. As noted earlier in section 6.4.2, there are several large-scale faults within the study area that play a significant role in the structural trapping of hydrocarbons. However, the capability of a fault to retain hydrocarbon columns does not preclude the potential for fault leakage, especially if formation pressures are increased as a result of CO_2 injection.

The *in situ* stress regime in the Barrow Sub-basin is estimated to be a strike-slip fault regime at the likely depth of injection (~2200 m), i.e. the maximum horizontal stress (S_{Hmax}) is greater than the vertical stress (S_v), which in turn is greater than the minimum horizontal stress (S_{hmin}) (Figure 6.34). However, this transitions to a normal fault stress regime ($S_v > S_{Hmax} > S_{hmin}$) or a regime at the boundary of normal to strike-slip faulting ($S_{Hmax} \approx S_v > S_{hmin}$) in the upper 1500 m of the study area (e.g. at Barrow Island) (Figure 6.34) (Streit, 2003). The orientation of the maximum horizontal stress is interpreted to be consistent with S_{Hmax} orientations determined by previous studies in the Northern Carnarvon Basin (090°N to 100°N) and an average S_{Hmax} direction of 095ºN was used in this analysis (Hillis & Williams, 1993; Hillis *et al.*, 1997; Streit, 2003).

The strike orientation of existing faults and their angle of dip with respect to the stress orientation and magnitude determine their potential for possible reactivation. Most of the major faults in the study area have east-northeast to northeast trends. This includes the Wonnich Fault and the Lowendal Fault system in the Harriet-Campbell area, both of which intersect the top of the potential storage formation at around 2 km depth, and the Barrow Island Fault, which intersects the top of the potential storage formation at around 1 km depth (detailed information on the geometry of some segments of the major faults were listed previously in Table 6.1). 2D failure plots were used to estimate the potential for fault reactivation, using the methodology of Streit (1999). The failure plots indicated that the

NOTE:
This figure is included on page 212 of the print copy of the thesis held in the University of Adelaide Library.

Figure 6.34 Stress and pressure profile for the Barrow Sub-basin. Estimate of minimum horizontal stress (S_{hmin}) was based on pressure data from leak-off tests. Estimate of the vertical stress (S_v) was obtained by integrating data from density logs. Estimate for the maximum horizontal stress (S_{Hmax}) was based on the occurrence of drilling-induced tensile fractures in Wonnich-1. A frictional limit for σ_1 is shown assuming cohesionless faults with a coefficient of friction of $\mu = 0.85$ (modified after Streit, 2003).

majority of the faults in the study area could potentially be reactivated in a strike-slip stress regime (or normal stress regime for the Barrow Fault) (Figure 6.35) (Streit, 2003). Although reactivation of some of the faults may be possible, this would only be induced if the appropriate pore fluid pressures required for failure were exceeded during injection. For such faults, maximum sustainable pore fluid pressures that will not cause fault reactivation can be estimated.

In cases where dip-angles of fault segments are known (Figure 6.36a), sustainable pore fluid pressures were estimated using the Fault Analysis Seal Technology (FAST) technique by Mildren et al (2002). Figure 6.36b shows a FAST polar plot for 2 km depth, applicable to the northern part of the study area with a target CO_2 storage depth of approximately 2 km. The FAST plot indicates that a pore pressure increase of approximately 7 MPa (1015 psi) could induce slip on faults. Given that hydrostatic pressure is about 20 MPa at 2 km depth, sustainable pore fluid pressures are estimated to be less than 27 MPa (< 3916 psi). Lower sustainable pore fluid pressures may result if the faults have lower frictional strength properties than assumed (cohesive strength C = 2 MPa, friction coefficient $\mu = 0.6$) (Streit, 2003).

Farther to the south, the Barrow Island fault intersects the top of the potential storage formation at approximately 1 km depth. For this depth (at which the fault geometry and

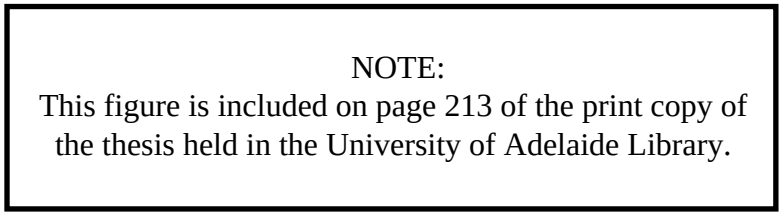

Figure 6.35 Map showing potential for fault reactivation at 2 km depth in a strike-slip stress regime (except Barrow Fault, which is 1 km depth in a normal stress regime): faults shown in blue are relatively stable and faults shown in red can possibly be reactivated. Arrow indicates approximate S_{Hmax} direction (modified after Streit, 2003).

SHmax magnitude are poorly constrained) a normal fault stress regime is indicated in Figure 6.34. FAST polar plots for 1 km depth are shown in Figure 6.36c and Figure 6.36d, and indicate that the Barrow Island fault is relatively close to failure. In Figure 6.36c the faults are assumed to have frictional properties similar to those used in Figure 6.36b; in Figure 6.36d the faults are assumed to be cohesionless and have a μ of 0.85, as inferred from Figure 6.34. A pore fluid pressure increase of only a few megapascals (2–5 MPa; 290–725 psi) is estimated to induce fault failure (Streit, 2003).

NOTE:
This figure is included on page 214 of the print copy of the thesis held in the University of Adelaide Library.

Figure 6.36 (a) Location of fault segments assessed with FAST polar plots shown in green. Numbers correspond to fault numbers shown in (b) to (d). (b) FAST polar plot indicating pore pressure increase required to induce fault reactivation at 2 km depth. Faults are shown as poles to planes. Assumed fault properties are C = 2 MPa and μ = 0.6. (c) and (d) FAST polar plots indicating pore pressure increase required to induce fault reactivation at 1 km depth. Faults are shown as poles to planes. Assumed fault properties in (c) are C = 2 MPa and μ = 0.6 and in (d) are C = 0 MPa and μ = 0.85 (modified after Streit, 2003).

The results of the geomechanical modelling indicate that both the major faults within the Barrow Island trend area could be susceptible to fault reactivation. Injection of CO_2 near the Wonnich Fault would need to be constrained at a rate that ensures pressure does not exceed

7 MPa (1015 psi) above hydrostatic pressure. As the reservoir quality of the Flag Sandstone is highly permeable, pressure should be able to disperse quite easily and excessive pressure build-ups are not expected to be a problem. The Barrow Island Fault requires much less pore pressure increase to induce fault reactivation. However, the Barrow Island Fault is about 40 km from the potential injection location, so it is unlikely that the pore fluid pressure would increase that much so far from the injection point. The estimates of maximum sustainable pore fluid pressure increases presented here are only guides rather than a definitive answer because of the number of assumptions included in the geomechanical modelling (particularly with respect to fault and host rock frictional properties). Additional geomechanical and petrophysical data will be required in order to provide more realistic estimates of maximum sustainable pore fluid pressures that will not induce brittle failure of faults or rocks in the Barrow Sub-basin.

6.7.5 Hydrodynamic Analysis of Formation Water Flow Systems

The existing formation water flow system within a geological reservoir may influence CO_2 migration pathways and containment, both in terms of the magnitude of the fluid movement and the direction. Hydrodynamic modelling was undertaken by Hennig *et al*. (2003) to assess the formation water flow systems operating within the Barrow Sub-basin.

The results of the hydrodynamic modelling indicate that the Flag Sandstone, Flacourt Formation and Malouet Formation behave as a single, hydraulically-connected unit, referred to herein as the Barrow Group Aquifer (Figure 6.4). The formation pressures obtained prior to production were converted to hydraulic head values, which are a measure of the fluid potential (mechanical energy per unit mass), and plotted as a potentiometric surface map of the aquifer (Figure 6.37). This indicates that the pre-production regional flow direction was predominantly from the sub-basin margins towards the centre, with an exit point proposed to the southwest. It also shows that the Lowendal Fault is a significant hydrodynamic flow barrier, with flow on the eastern (Harriet) side directed to the northeast and flow on the western (Bambra) side directed to the southwest. However, the potentiometric contours show convergence at the southern end of the Lowendal Fault, which may indicate the existence of a hydraulic pathway across the fault, via a sand-on-sand juxtaposition below the oil-water contact at Harriet (Hennig *et al.*, 2003). The pre-production flow velocity for the study area is calculated at 19.5 cm/year (using an average permeability of 600 mD) (Hennig *et al.*, 2003).

The general direction of the pre-production formation water flow in the Barrow Island

Figure 6.37 Potentiometric surface map for the Barrow Group Aquifer prior to aquifer-sourced hydrocarbon production. Green arrows indicate formation water flow direction (modified after Hennig *et al.*, 2003).

trend area is towards the northwest, almost opposite to the predicted CO_2 migration pathway based on structural geometry and buoyancy drive. Therefore, had there been no fluid production in the region, the opposing aquifer drive could have helped to slow the migration of the injected CO_2 along the axis of the Barrow anticline. However, the removal of large volumes of fluid by hydrocarbon and water production has affected the aquifer pressure and the rate and direction of formation water movement. Hydrocarbon production from the Flag Sandstone commenced in 1986 with the Harriet Field, and water has been produced from the Flacourt Formation at Barrow Island (for re-injection into the Windalia Sandstone Member) since 1967. The hydraulic head values have decreased over time, indicating that the fluid

removal rate is greater than the recharge rate; hence, pressure in the Barrow Group Aquifer is declining because of the fluid production (Hennig et al., 2003).

The impact of production in the area was superimposed on the pre-production flow system to quantify the effects of removal of large volumes of fluid in terms of changes in formation water flow velocity and direction. The large volumes of water produced from the Flacourt Formation have had limited impact, with a predicted maximum drawdown of 6 m hydraulic head, equivalent to 0.06 MPa (9 psi), up to 20 km away from the centre of Barrow Island (Figure 6.38) (Hennig *et al.*, 2003). In contrast, production from the Harriet Field appears to have had a significant impact, creating a hydraulic low centred over the Harriet Field and a predicted drawdown of 30 m hydraulic head, equivalent to 0.3 MPa (43 psi), at approximately 20 km away (Figure 6.38) (Hennig *et al.*, 2003). The effects of pressure depletion at the Harriet Field have been transmitted as far northwest as the Wonnich Field, most likely via the hydraulic pathway identified at the southern end of the Lowendal Fault. The original formation water flow direction has been altered and now flows towards the hydraulic low at the Harriet Field. In addition, the flow velocity has increased to 30 cm/year (assuming an average permeability of 600 mD) (Hennig *et al.*, 2003).

The production-induced pressure decline and change in formation water flow direction and velocity may impact on the predicted buoyancy-driven CO_2 migration pathway. The pressure decline is a transient effect; however, aquifer recovery is not likely to occur prior to the initiation of CO_2 geological storage, so the present-day conditions need to be considered. Instead of CO_2 migrating up-dip southwards along the axis of the Barrow anticline, it could be diverted down-dip towards the southeast by the pressure drawdown in the vicinity of the Harriet Field. Whether this is a likely scenario depends on the relative strengths of the up-dip buoyancy driving force versus the down-dip hydraulic driving force.

A tilt analysis was conducted to determine if formation water flow is likely to be a significant factor in determining the migration direction of CO_2 in the aquifer. The methodology followed is that presented by Underschultz and Johnson (2005). The local tilt of a CO_2-water interface is determined by the ratio of the fluid densities of CO_2 (ρ_{CO2}) and water (ρ_w), and the hydraulic gradient (*GradH*; rate of change of the hydraulic head over a given horizontal distance), as shown by Equation 12 (Underschultz & Johnson, 2005):

$$Tilt = GradH \times \frac{\rho_w}{(\rho_w - \rho_{CO2})} \quad [12]$$

Figure 6.38 Approximate radius of production-induced pressure drawdown for the Barrow Island and Harriet fields. Green arrows indicate formation water flow direction (modified after Hennig *et al.*, 2003).

Assuming a CO_2 injection site just to the south of the Wonnich Field (depth 2150 m) and using the pressure, temperature and salinity relationships defined earlier in section 6.2.2, water density (ρ_w) is 1.0061 g/cm^3 and CO_2 density (ρ_{CO2}) is 0.6567 g/ cm^3. The hydraulic head decreases from the Wonnich injection site southeastward towards Harriet by about 40 m. Across a distance of 20 km, this defines a hydraulic gradient (*GradH*) of 0.002 m/m dipping to the southeast and a tilt to the CO_2-water interface of 0.006 m/m. The structural gradient to the southeast is 0.01 m/m (200 m across 20 km). Therefore, on the basis of this tilt analysis the hydrodynamic driving force is not likely to be strong enough to bring the CO_2 down-dip towards Harriet. However, it may deflect the migration path towards the southeast more than

what is expected from buoyancy drive alone.

6.8 CAPACITY

To assess the CO_2 storage capacity, a 3D geological model was created from the structural and stratigraphic interpretations. The zones and layers of the model were constructed to reflect the internal stratigraphic architecture of the geological units seen on the seismic (Figure 6.39). The 3D cellular grids were then populated with reservoir parameters derived from the petrophysical assessment (e.g. sand percent, porosity, permeability) using sequential Gaussian simulation (Figure 6.40). Other physical parameters important to the behaviour of CO_2 (e.g. pressure, temperature) were also populated in the model. The cellular 3D geological models also provided the basis for the numerical flow simulation models of CO_2 injection and storage created during the engineering characterisation.

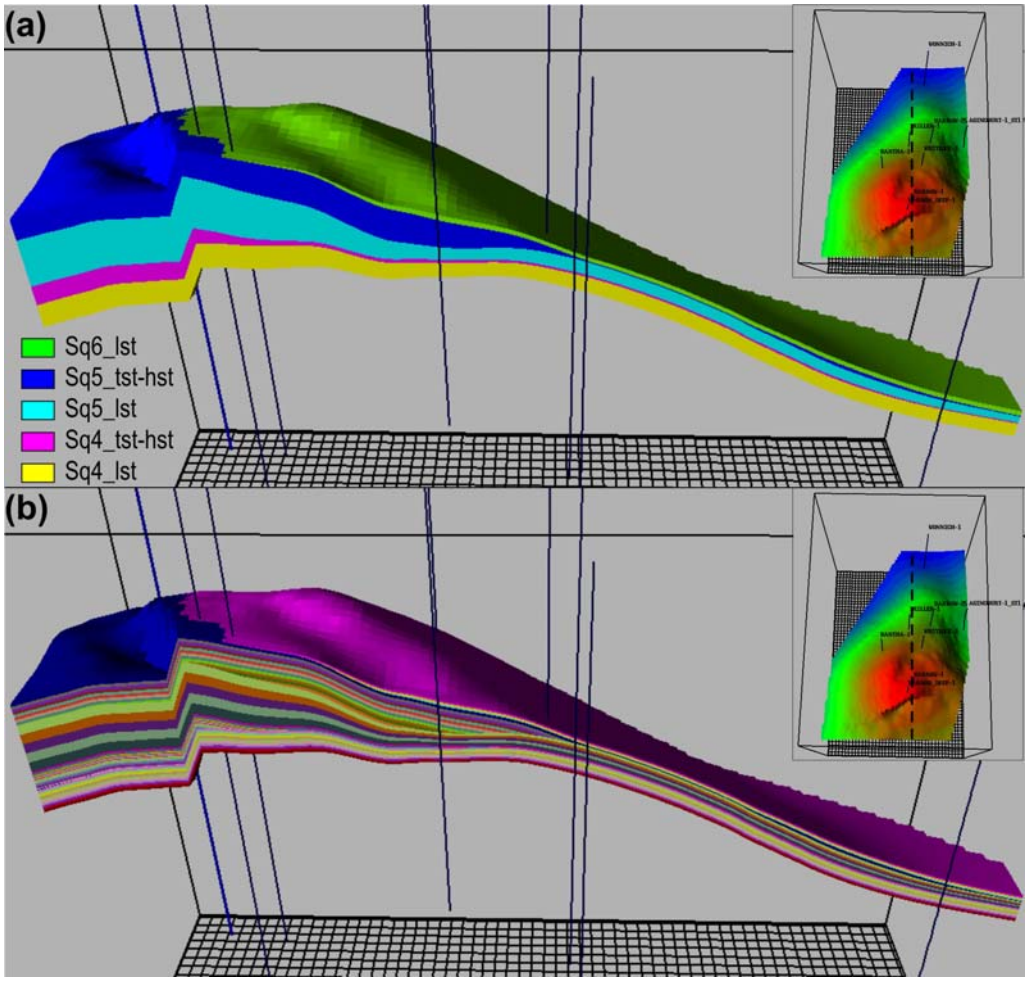

Figure 6.39 South-north cross-section through the Barrow Island anticline 3D geological model, showing the distribution and geometries of the (a) zones and (b) layers constructed within the model. Inset maps show the base Muderong Shale depth structure surface (ts6), with the dashed line indicating the location of the cross-sections.

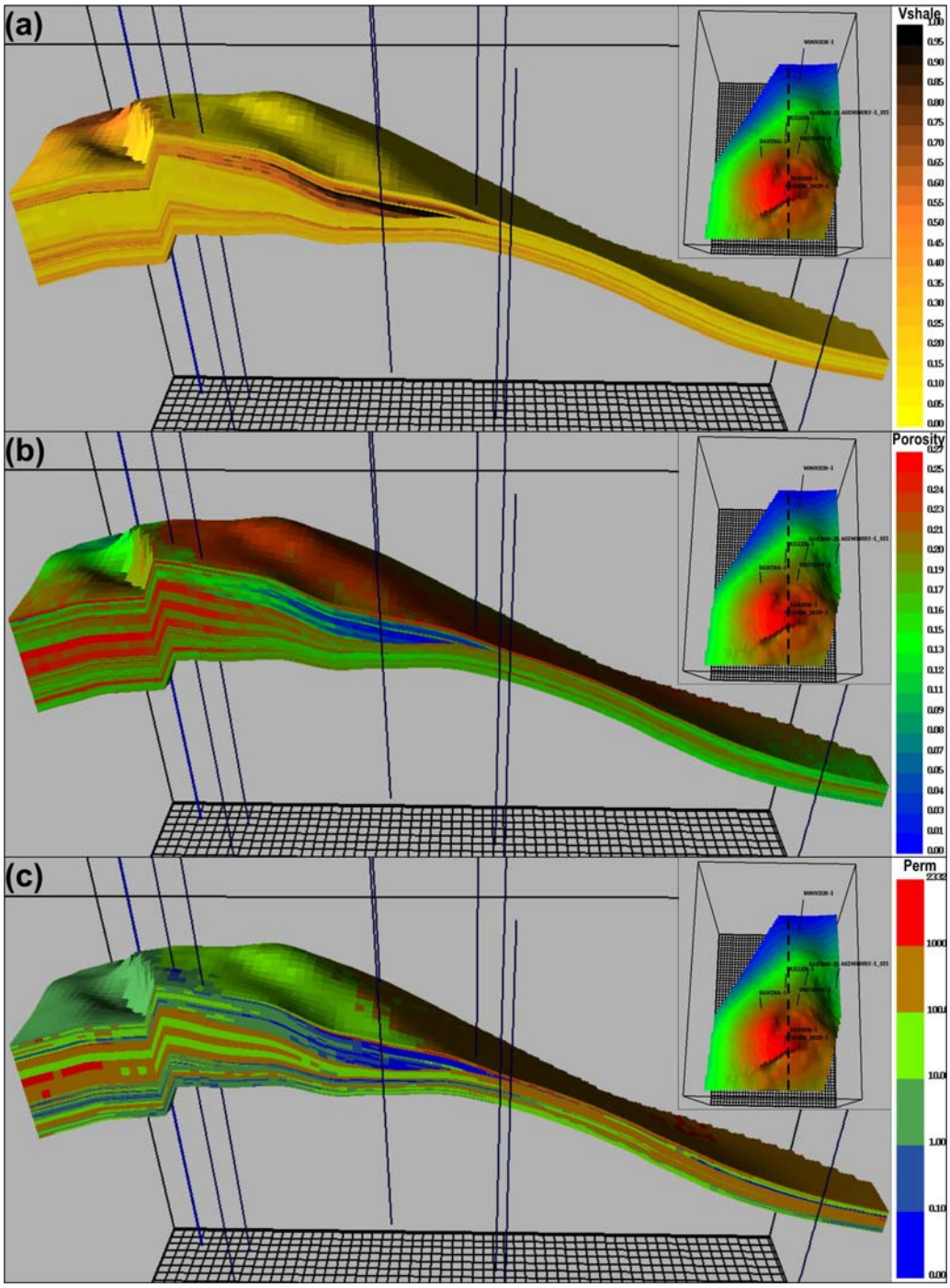

Figure 6.40 South-north cross-section through the Barrow Island anticline 3D geological model, showing one realisation of (a) volume of shale, (b) porosity and (c) permeability. Inset maps show the base Muderong Shale depth structure surface (ts6), with the dashed line indicating the location of the cross-sections.

The results of the volumetric assessment for potential CO_2 storage capacity in the Muderong Shale Subcrop ESSCI are presented in Table 6.5. The Flag Sandstone in its entirety has considerable pore space available for the storage of CO_2. However, not all of that available pore volume will be accessed by the CO_2 due to its buoyant nature. After initial

accumulation around the injection well, the CO_2 is likely to rise to the top of the reservoir and spread out in thin layers beneath the intraformational seals or Muderong Shale regional seal. The storage efficiency factors of DOE (2007) account for such factors as net to total area, net to gross thickness, effective to total porosity, areal displacement efficiency, vertical displacement efficiency, gravity, and microscopic displacement efficiency. If these factors of 1–4 % are applied to the available pore volume, the potential storage capacity is still in the order of hundreds to thousands of Mt of CO_2.

A potential source of CO_2 for this site would be an estimated 1.5 TCF from the Burrup Peninsula gas and LNG processing plants and 2.0 TCF from the potential Gorgon Field development over a 20-year period (Bradshaw *et al.*, 2002), totalling 3.5 TCF (185.7 Mt). Therefore, on the basis of the static CO_2 storage capacity estimates, the Barrow Island trend area can easily accommodate the possible source volumes. Dynamic numerical simulations of CO_2 sweep through the reservoir conducted as part of the engineering characterisation will determine more realistic CO_2 storage capacity estimates.

Table 6.5 CO_2 storage capacity volumetric assessment for reservoir zones within Muderong Shale Subcrop ESSCI.

Zone	Pore Volume (m^3)	CO_2 Volume (m^3)	Total CO_2 (TCF)	Total CO_2 (Mt)†	E = 1% CO_2 (Mt)	E = 4% CO_2 (Mt)
Sq6_lst	5,875,248,640	1,516,868,993,024	54	2,843	28	114
Sq5_lst	41,232,867,328	10,406,193,004,544	368	19,501	195	780
Sq4_lst	27,983,335,424	7,689,758,310,400	272	14,569	146	583
Total	*75,091,451,392*	*19,612,820,307,968*	*693*	*36,913*	*369*	*1,477*

† Conversion factor of 1 TCF = 53.0657705140448 Mt at standard temperatures and pressures (14.65 psia and 60ºF surface conditions).

6.9 POTENTIAL IMPACT ON EXISTING NATURAL RESOURCES

The Flag Sandstone is a major hydrocarbon reservoir unit within the Barrow Sub-basin. Numerous oil and gas accumulations exist within this stratigraphic unit at various different stages of development and production. By injecting south of the Wonnich Field, CO_2 storage could be accomplished without compromising these natural resources. As the Flag Sandstone is still a promising hydrocarbon exploration target, the risks of potential resource contamination and the economical risks of this operation would need to be carefully evaluated prior to any injection of CO_2 in the Barrow Sub-basin.

6.10 CONCLUSIONS

The Flag Sandstone and its lateral equivalents within the Early Cretaceous succession of the Barrow Sub-basin were assessed for their suitability for geological storage of CO_2. The detailed geological site characterisation process involved an interpretation of the geological structure, stratigraphic fill, reservoir and seal properties, petrography, geomechanics and hydrodynamics. The integration of all the various interpretations has yielded numerous results pertinent to the suitability of the Early Cretaceous succession in the Barrow Sub-basin as a potential site for geological storage of CO_2. The main outcomes are as follows:

- The structural geometry of the Early Cretaceous sediments in the Barrow Island area is a large, fault-bound, northward-plunging anticline. Faulting intensity is low but the faults that do occur are large-scale normal faults. In the area of interest, the Wonnich Fault and the Barrow Island Fault intersect the anticlinal structure 40 km apart.
- The stratigraphic fill reflects several relative sea level changes and seven unconformity-bound sequences were identified from the base Cretaceous to the top Muderong Shale. The clastic depositional environments identified were all fully marine, ranging from deep basin floor to mid shelf.
- The reservoir units of the Flag Sandstone (Sequences 4 to 6) are characterised by thick (~225m), laterally extensive (~2,250 km^2), stacked, amalgamated basin floor fan lobes, which are likely to have an overall excellent degree of interconnectivity. At basin-scale, the hydrodynamic regime indicates that the Flag Sandstone and its lateral equivalents operate as a single connected aquifer (Barrow Group Aquifer System); however, compartmentalisation may occur at the field-scale due to the presence of thin hemipelagic shales in between individual fan lobes.
- Reservoir quality is very good. About three-quarters of the Flag Sandstone consists of medium to very coarse-grained massive sandstones, which have an average porosity of 21 % and permeability of 1343 mD, indicating that the Flag Sandstone has exceptionally high reservoir quality for CO_2 injection. Whilst some feldspar dissolution is possible, the subarkose mineralogy is unlikely to promote CO_2-water-rock interactions at a rate that could affect injectivity.
- The Muderong Shale seal (Sequences 6 to 7) above the Flag Sandstone is a very thick (~700 m), regionally extensive (>4,500 km^2) deep marine mudstone. It has excellent seal capacity (average CO_2 column height retention of 705 m) and is the proven seal for several oil and gas fields within the Barrow Sub-basin. Therefore, the seal

properties of the Muderong Shale are likely to provide secure containment for CO_2 storage.

- The likely migration pathway of CO_2 injected in a site south of the Wonnich Field is up-dip towards the south and Barrow Island along the axial trend of the anticline. Hemipelagic shale drapes within the Flag Sandstone may hinder or slow the vertical migration of CO_2 within the reservoir due to their high seal capacity (average CO_2 column height of 685 m). The trapping mechanisms for the containment of CO_2 are likely to be a combination of residual and solubility trapping along the migration pathway, stratigraphic trapping created by the hemipelagic shales drapes and by the interfingering of basin floor fan sandstones with up-dip continental slope shales, plus structural trapping within the fault-bound anticlinal closure at Barrow Island.
- Production-induced pressure decline has altered the *in situ* formation water flow direction towards a hydraulic low centred over the Harriet Field. The impact this may have on the predicted CO_2 migration pathway, however, is likely to be insignificant, as the buoyancy drive created by the upward-dipping structure is stronger than the hydrodynamic driving force.
- Fault reactivation of the east-northeast-trending major faults is possible within the inferred stress regime. However, this would only occur if injection pressures were not appropriately managed. Sustainable formation pressures that will not cause fault reactivation are estimated to be less than 27 MPa at an injection depth of ~2 km (i.e. an increase of 7 MPa above hydrostatic pressure).
- The potential CO_2 storage capacity is excellent, in the order of hundreds to thousands of Mt of CO_2. The Barrow Island trend area could easily accommodate possible source volumes from the Burrup Peninsula and Gorgon Field development if required.
- Since the Flag Sandstone is a major hydrocarbon reservoir unit within the Barrow Sub-basin, the risk to potential resource contamination would need to be carefully evaluated. However, an injection site to the south of the Wonnich Field could provide safe containment of CO_2 without potentially comprising any existing hydrocarbon resources.

In conclusion, the Barrow Sub-basin case study provides an example of CO_2 storage potential within the saline-leg of an active hydrocarbon system, where both stratigraphic and structural trapping components are important. The geological site characterisation has determined that the proposed Flag Sandstone reservoir is sufficiently porous and permeable to

allow injection of supercritical CO_2, that the overlying Muderong Shale seal provides effective containment, and that its size is large enough to provide storage capacity for nearby CO_2 sources. Therefore, the Early Cretaceous succession in the Barrow Sub-basin is likely to be a suitable candidate for geological storage of CO_2.